CONSTRAINING THE NEUTRON STAR EQUATION OF STATE WITH GRAVITATIONAL WAVE OBSERVATIONS

NIKOLAOS STERGIOULAS

DEPARTMENT OF PHYSICS
ARISTOTLE UNIVERSITY OF THESSALONIKI

NTUA, March 27, 2018

GW170817: The First Binary Neutron Star Merger

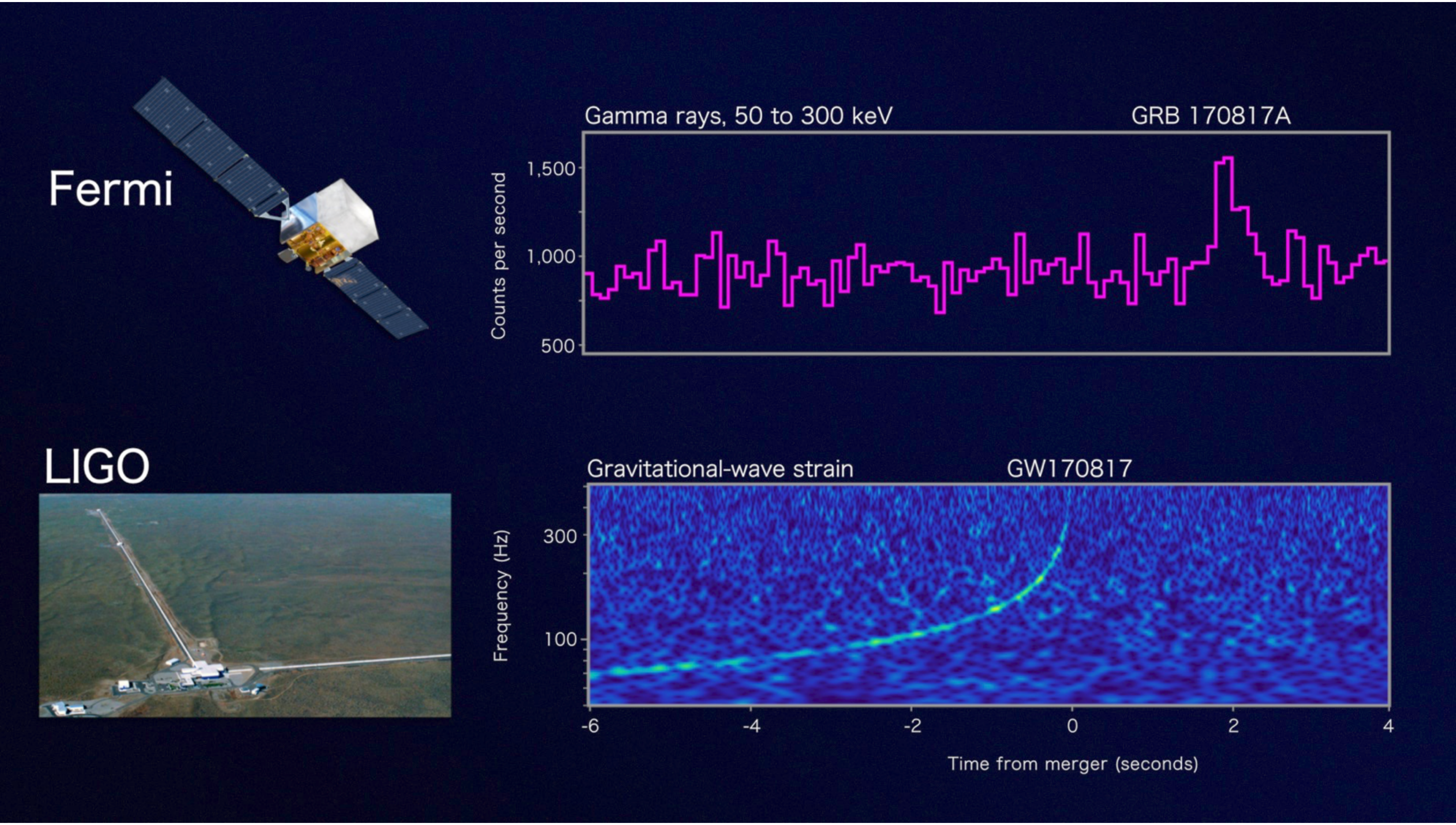

The First Binary Neutron Star Merger

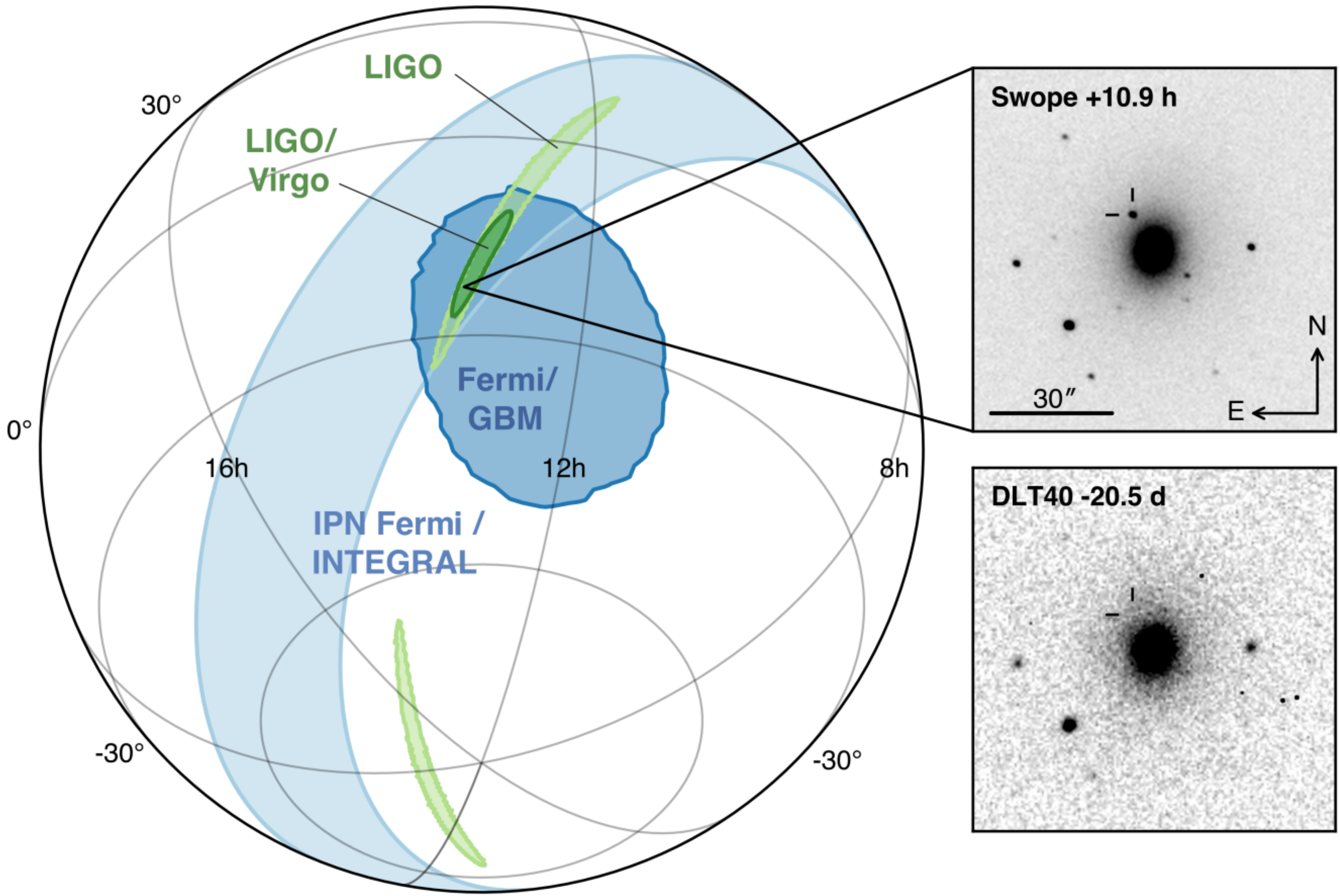

Interior Structure

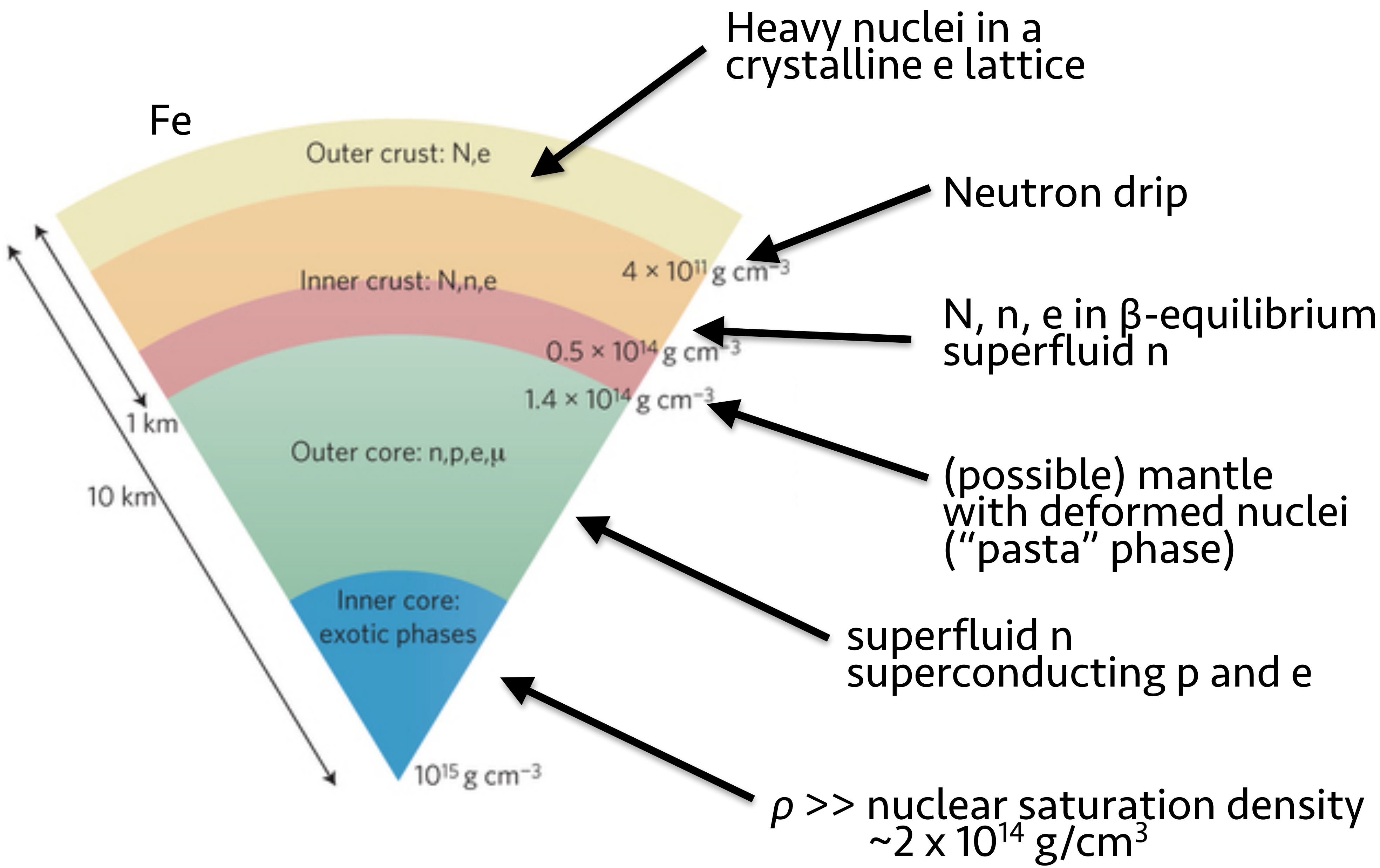

Equation of State (EOS)

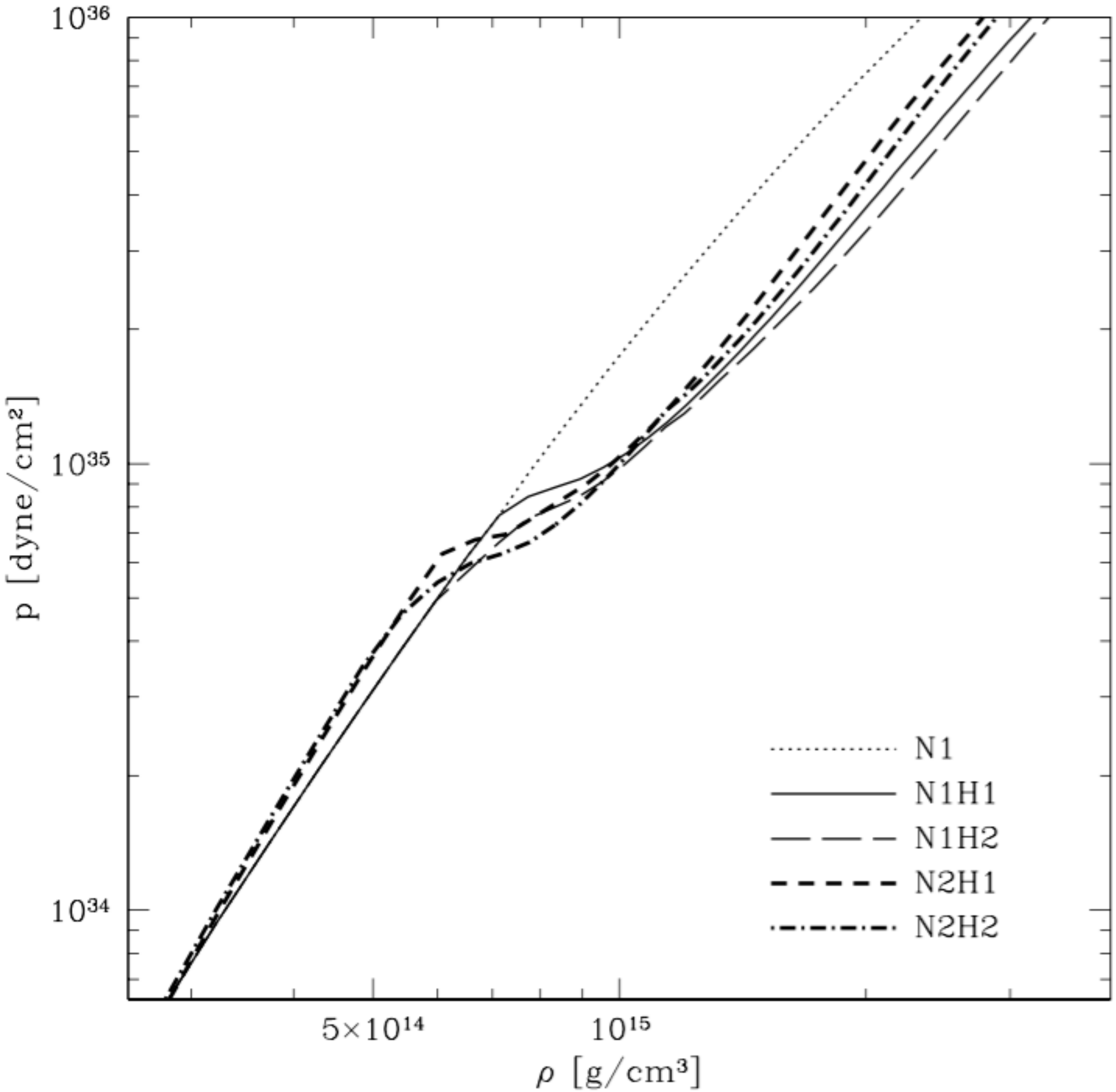

Hyperon = baryon (i.e. hadron + fermion) made of 3 quarks, with at least one strange quark:

- $\Lambda_0 = uds$
- $\Sigma^- = dds$
- $\Xi^0 = uss$
- etc...

Should appear at high density ($\rho > 2\rho_{\rm nuc}$)
$\Rightarrow$ EOS softening

N1 = np, N1H1,N2H1 = npΛΣ,
N1H2,N2H2 = npΛΣΞ
Balberg & Gal (1997)

(E. Gourgoulhon)

Different Possible Structures

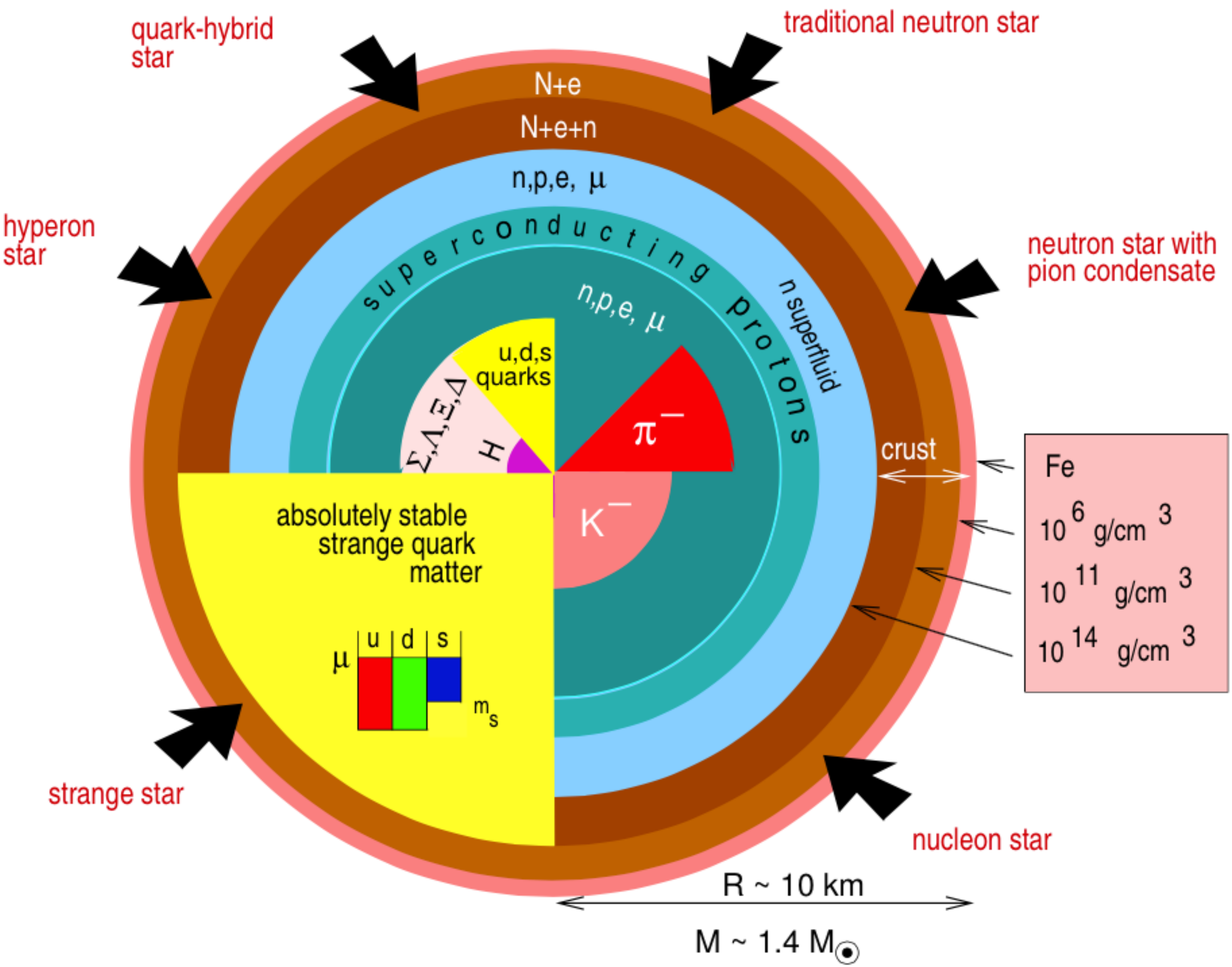

[Weber, J. Phys. G **27**, 465 (2001)]

Sample of Neutron Star Equations of State

Bauswein, Janka, Hebeler & Schwenk (2012)

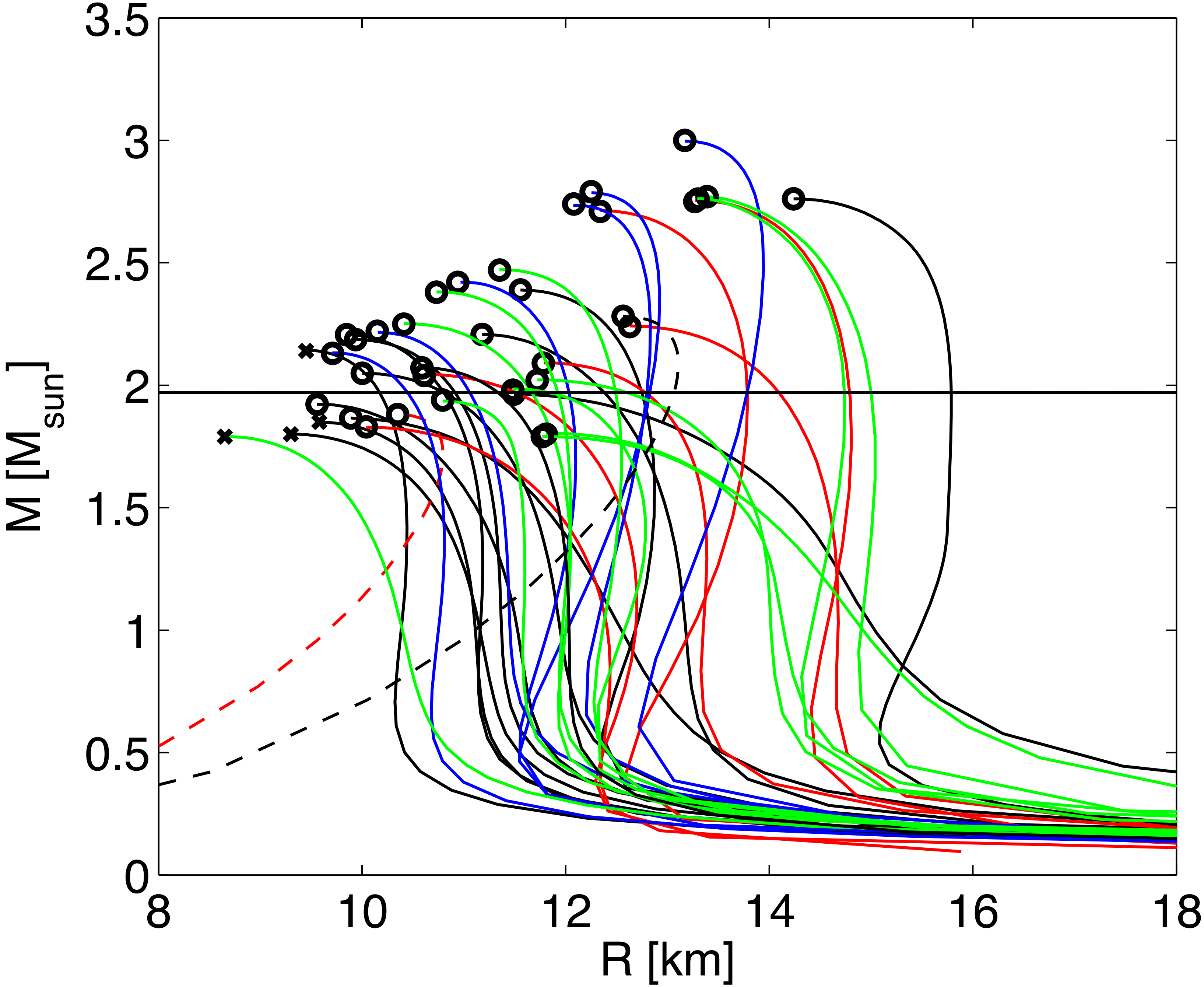

Sample of Neutron Star Equations of State

Bauswein, Janka, Hebeler & Schwenk (2012)

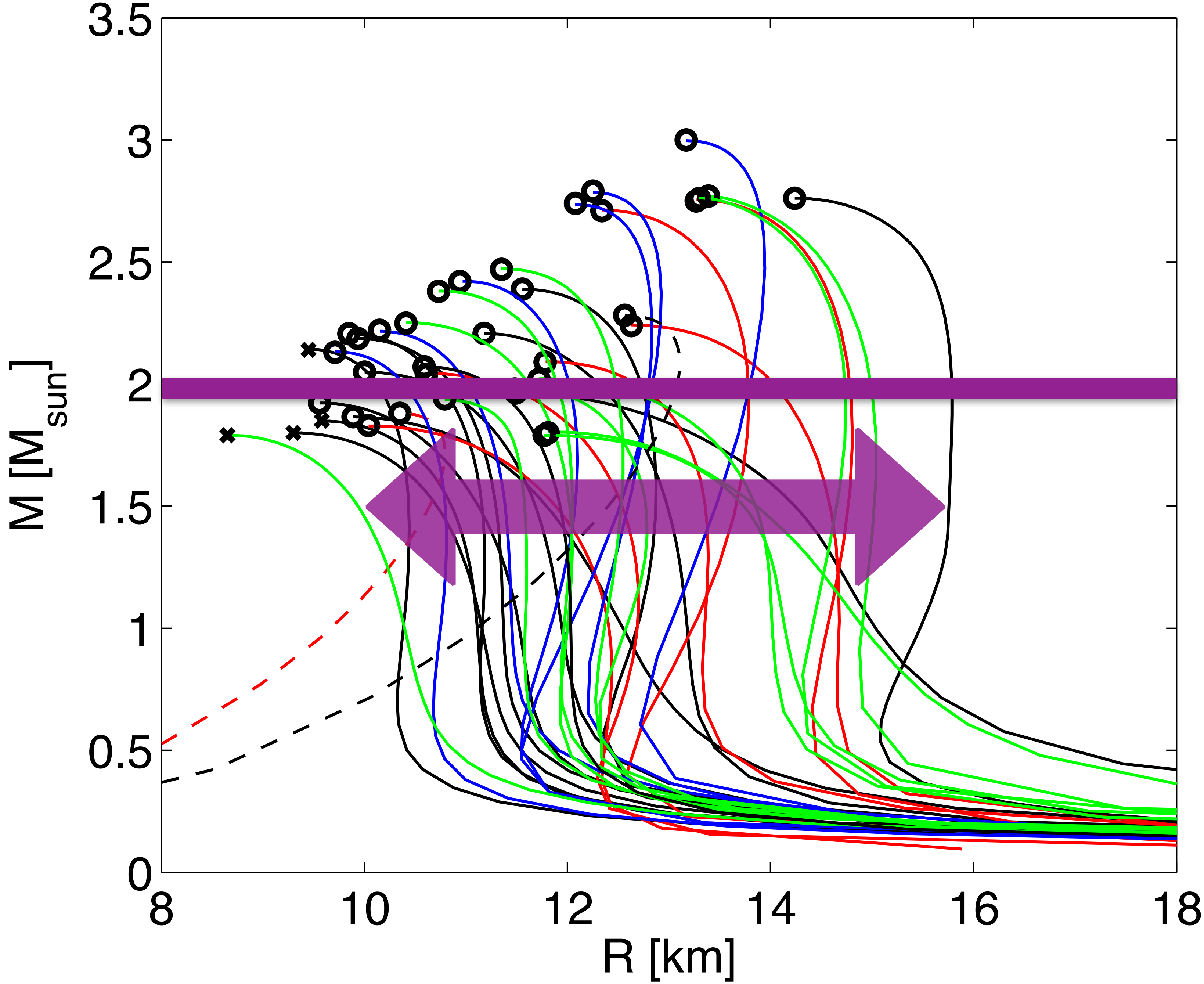

Maximally-Compact EOS

Koranda, NS & Friedman (1997)

Assume that the speed of sound is equal to the speed of light throughout the star ($v_s = c$):

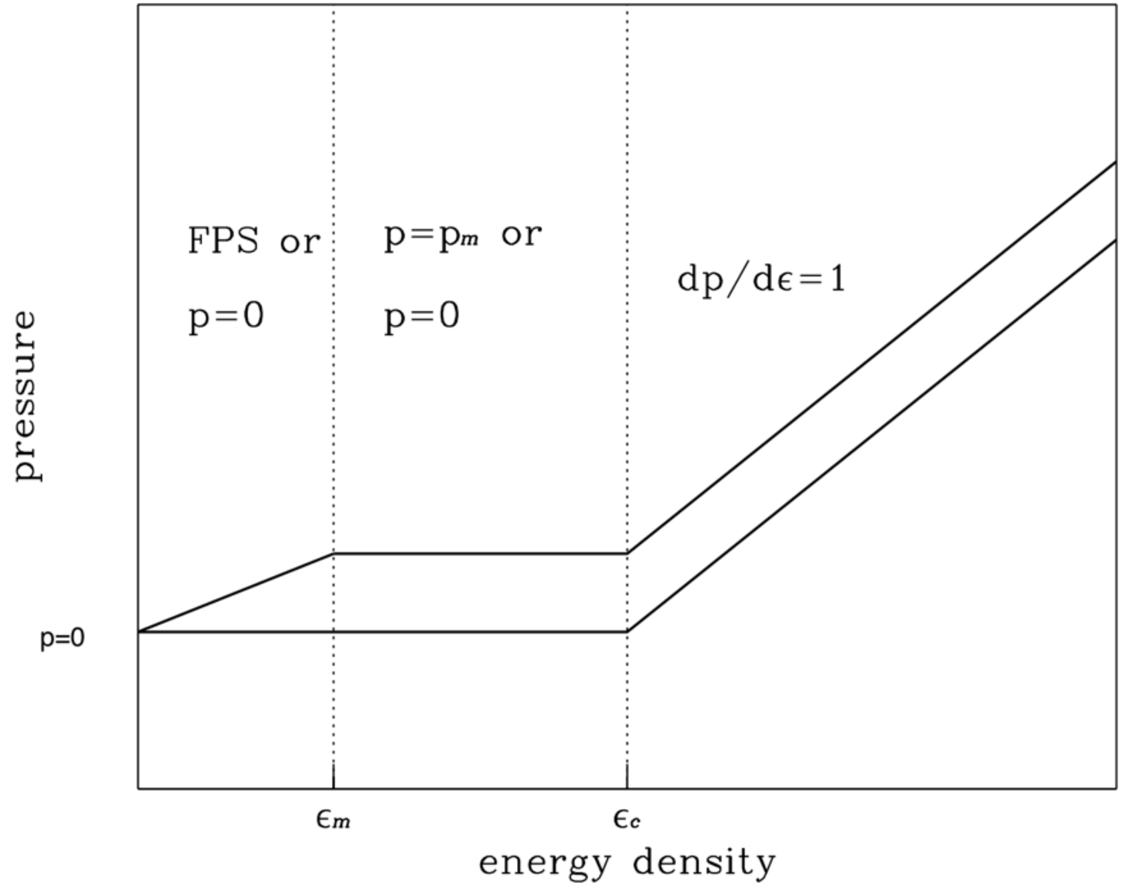

$$p(\epsilon) = \begin{cases} 0 & \epsilon \leq \epsilon_C \\ \epsilon - \epsilon_C & \epsilon \geq \epsilon_C \end{cases}$$

Maximally-Compact EOS Constraints

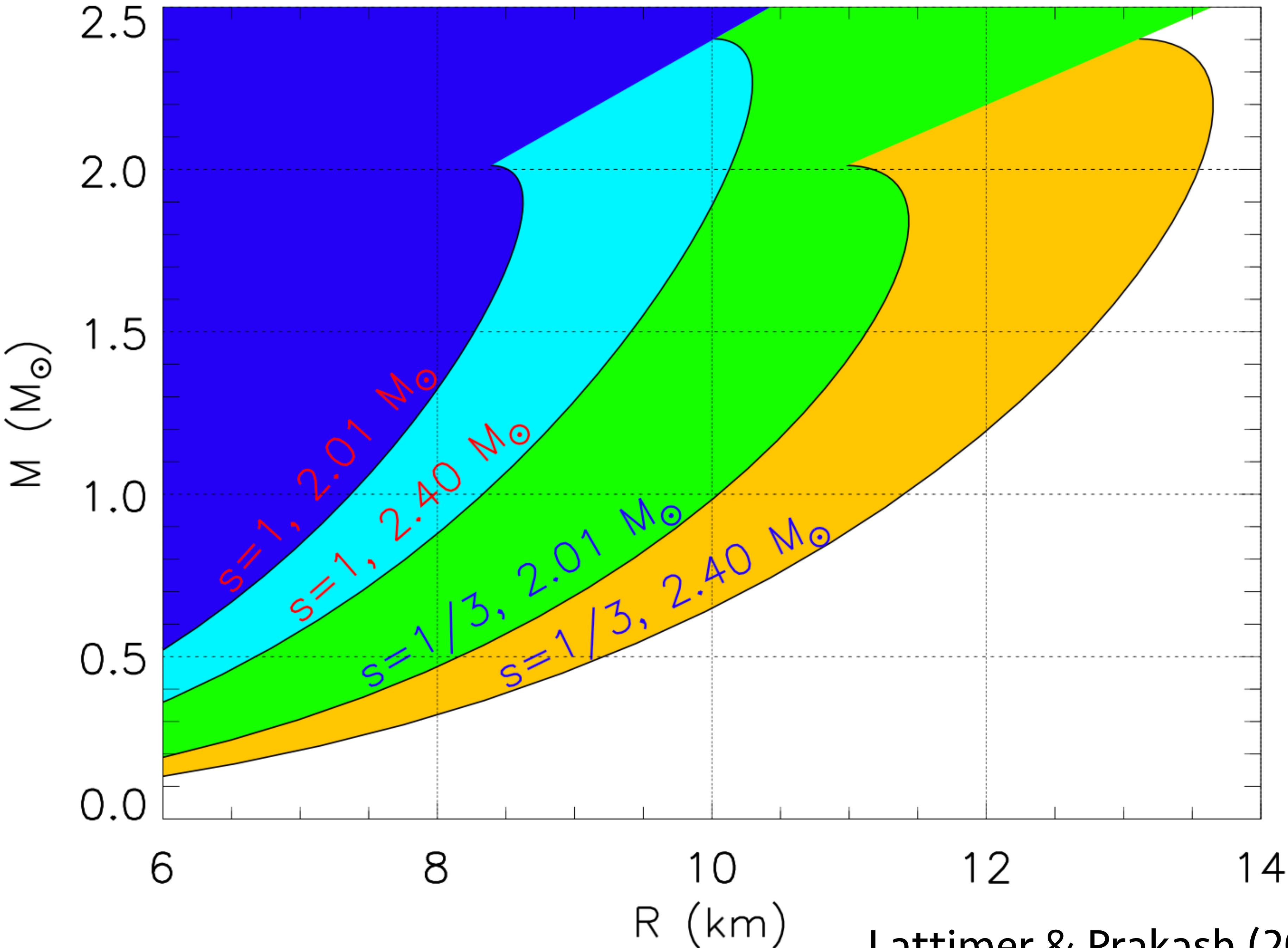

Lattimer & Prakash (2016)

Maximally-Compact EOS Constraints

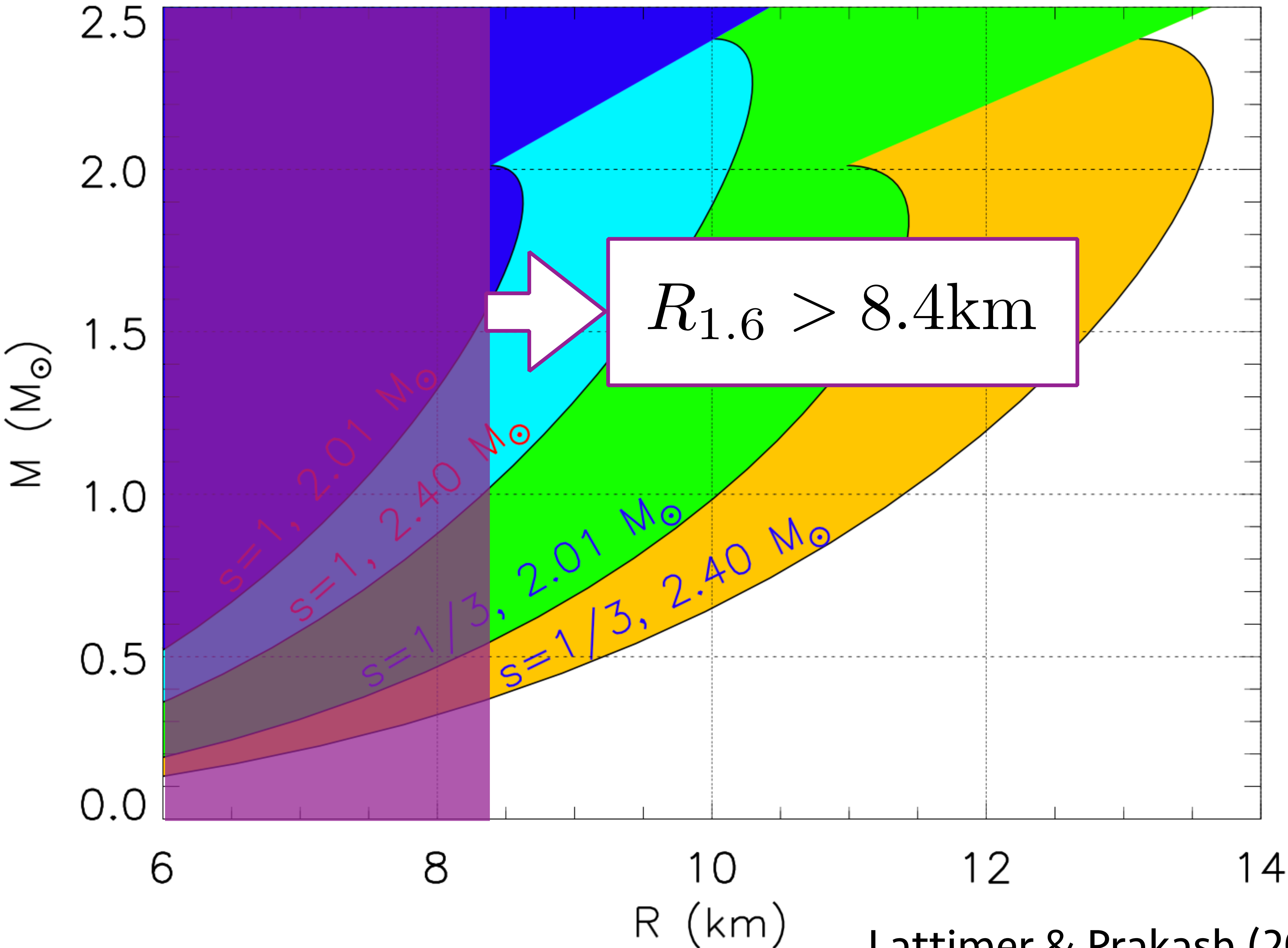

Lattimer & Prakash (2016)

Outcome of Binary NS Mergers

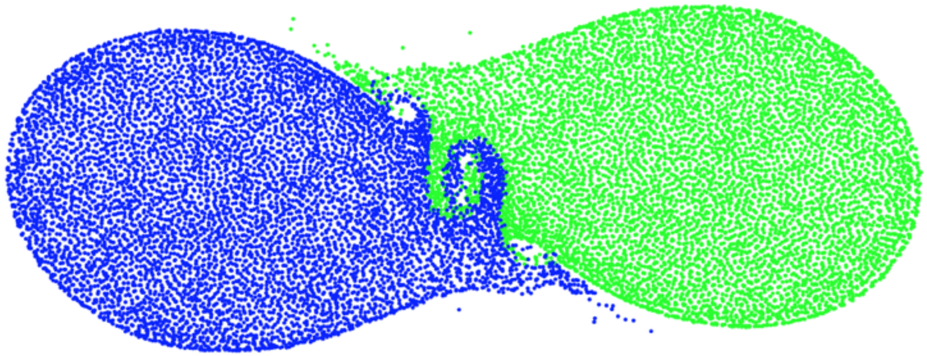

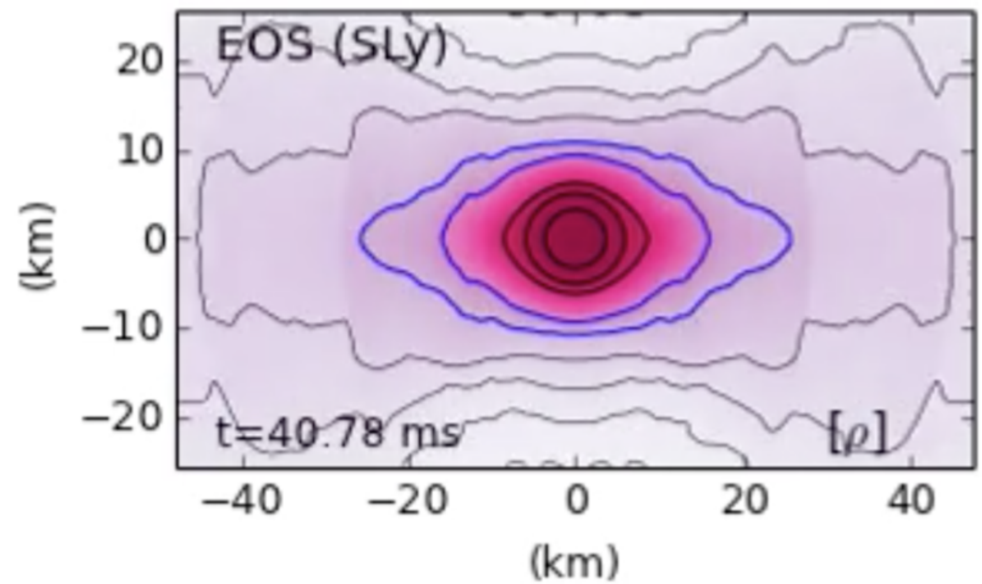

Most likely range of total mass for binary system:

$$2.4M_\odot < M_{\rm tot} < 3M_\odot$$

Because nonrotating $M_{\rm max} > 2M_\odot$ (as required by observations), a long-lived (τ >10ms) remnant is likely to be formed.

The remnant is a hypermassive neutron star (HMNS), supported by differential rotation, with a mass larger than the maximum mass allowed for uniform rotation.

Differentially Rotating Models

(Bauswein & NS 2017)

hypermassive stars

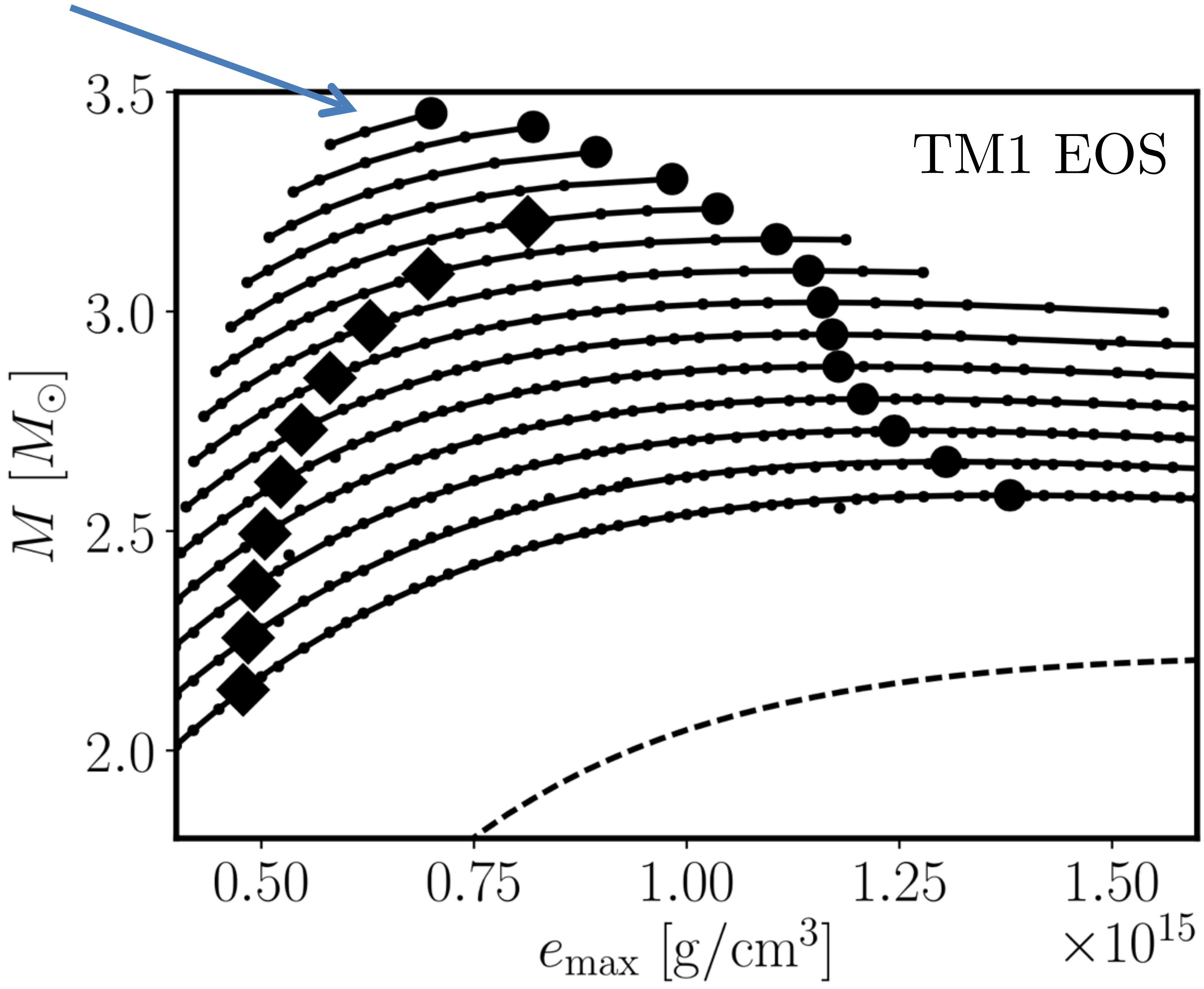

Differentially Rotating Models

(Bauswein & NS 2017)

hypermassive stars

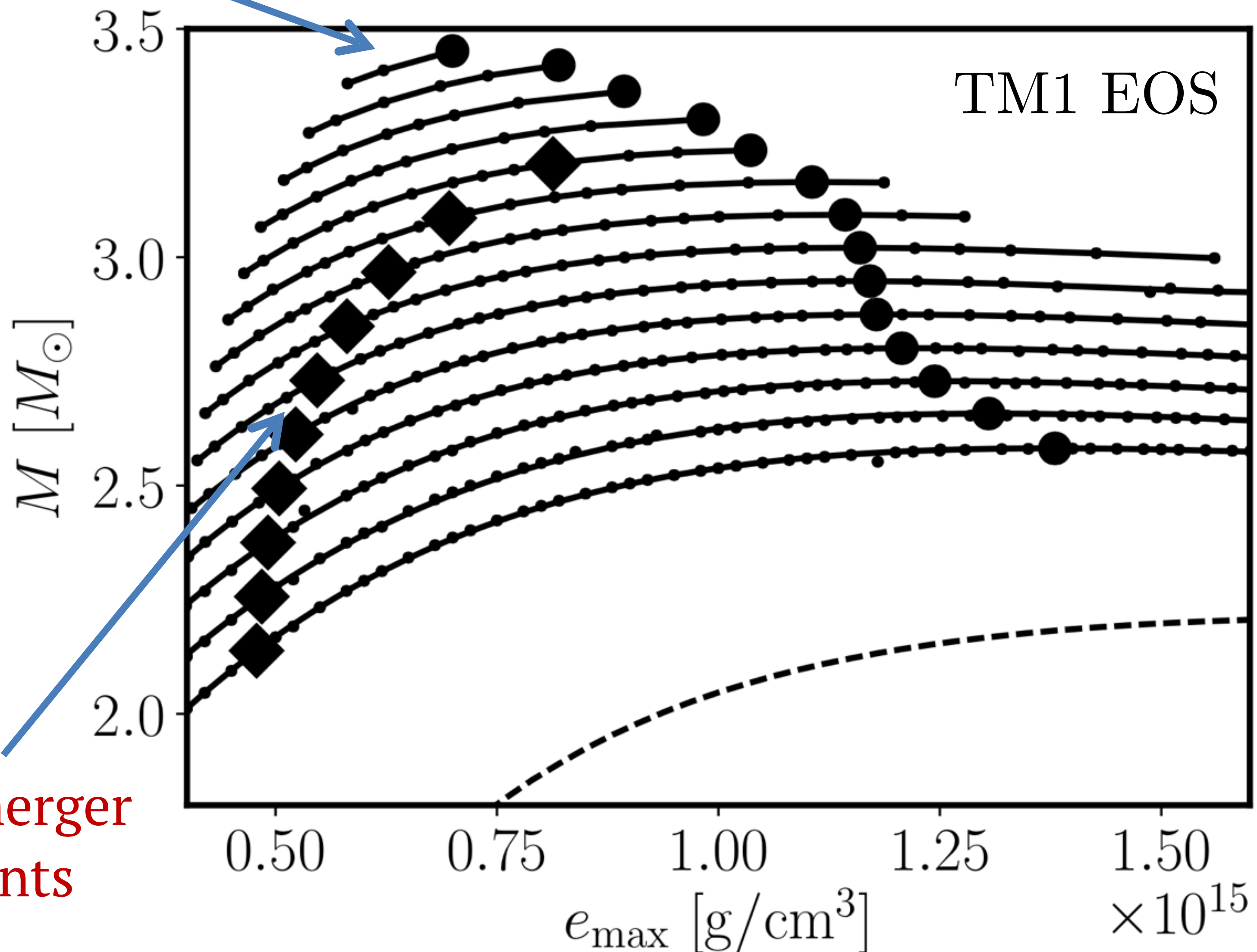

BNS merger remnants

universal relation!

Differentially Rotating Models

(Bauswein & NS 2017)

hypermassive stars

Threshold mass

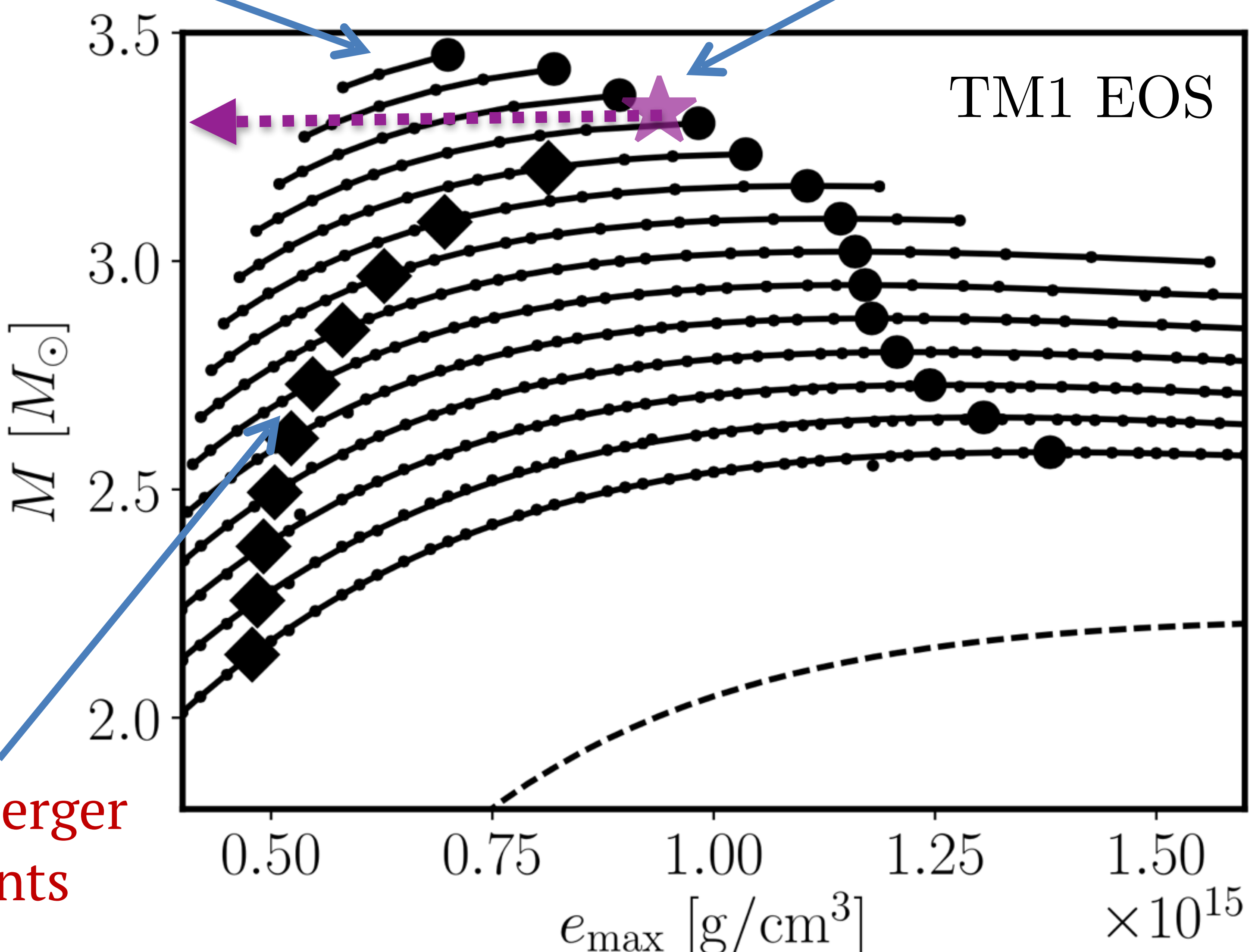

BNS merger remnants

universal relation!

Differentially Rotating Models

(Bauswein & NS 2017)

hypermassive stars

Threshold mass

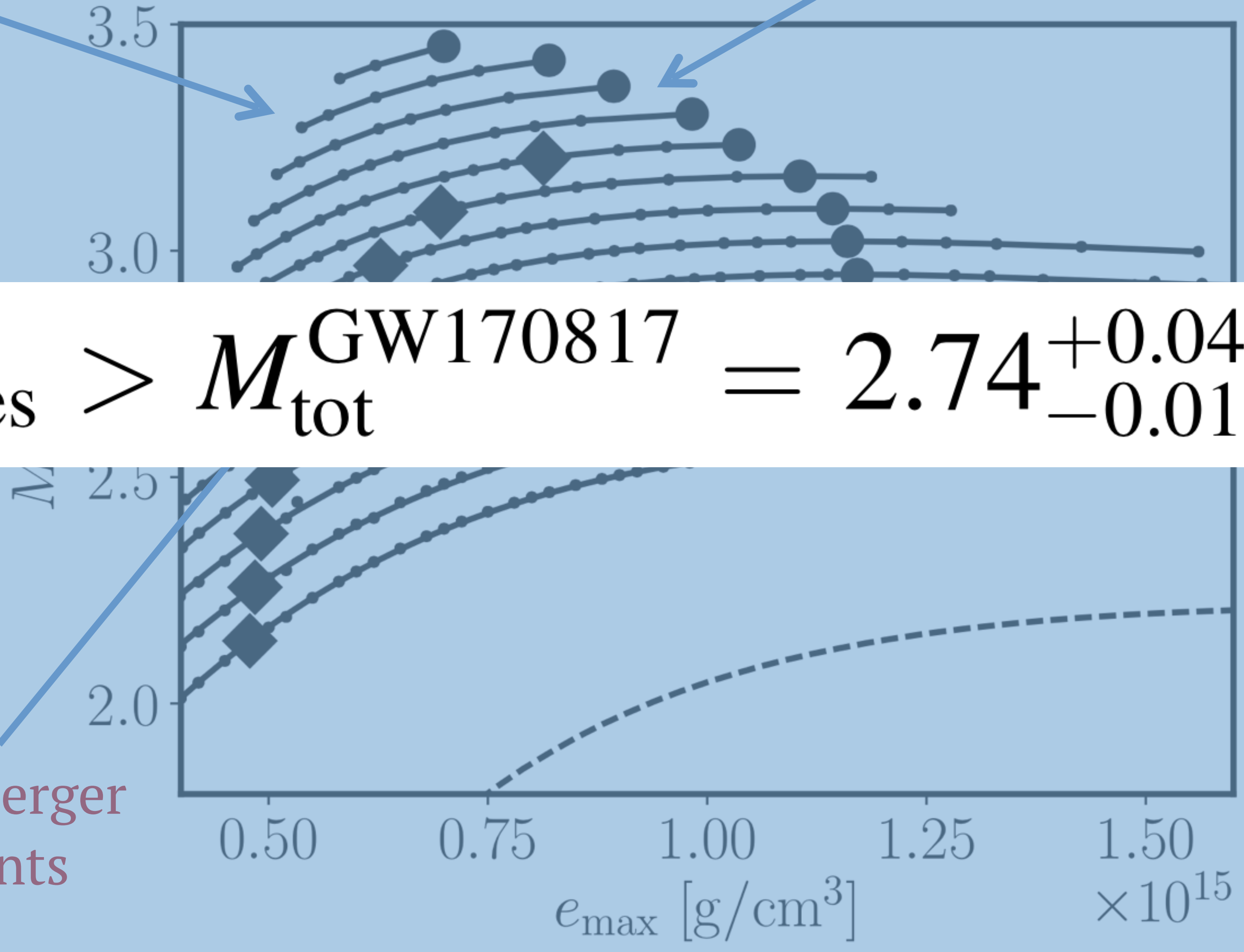

$$M_{\rm thres} > M_{\rm tot}^{\rm GW170817} = 2.74^{+0.04}_{-0.01}\, M_\odot$$

BNS merger remnants

M_thres vs. M_max correlation

Bauswein, Baumgarte, Janka PRL (2013)

The threshold mass is related to the maximum TOV mass as

$$M_{\mathrm{thres}} = k(C_{\mathrm{max}}) \cdot M_{\mathrm{max}} \qquad C_{\mathrm{max}} = \frac{M_{\mathrm{max}}}{R_{\mathrm{max}}}$$

where *k* is dependent on the compactness.

$$M_{\mathrm{thres}} = \left(-3.606\frac{GM_{\mathrm{max}}}{c^2 R_{1.6}} + 2.38\right) \cdot M_{\mathrm{max}}$$

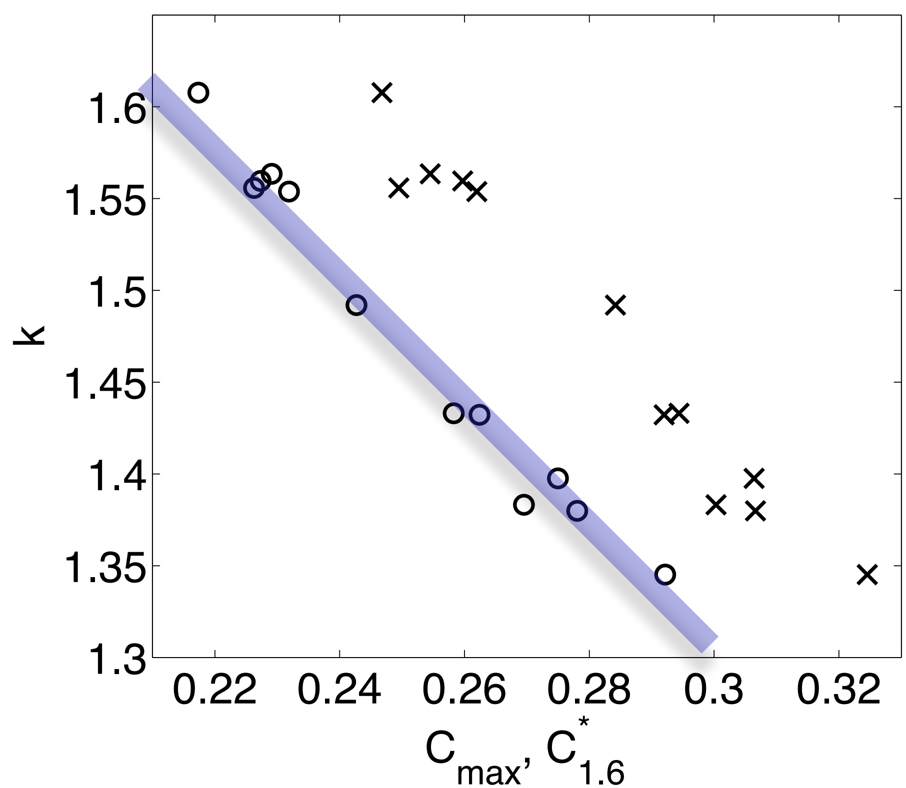

FIRST RADIUS CONSTRAINTS FROM GW's

Bauswein, Just, Janka, NS - ApJ Letters (2017)

Assume that each EOS is *maximally compact* above the density for 1.6 M_{sun} and combine with M_{thres}> 2.74 M_{sun}

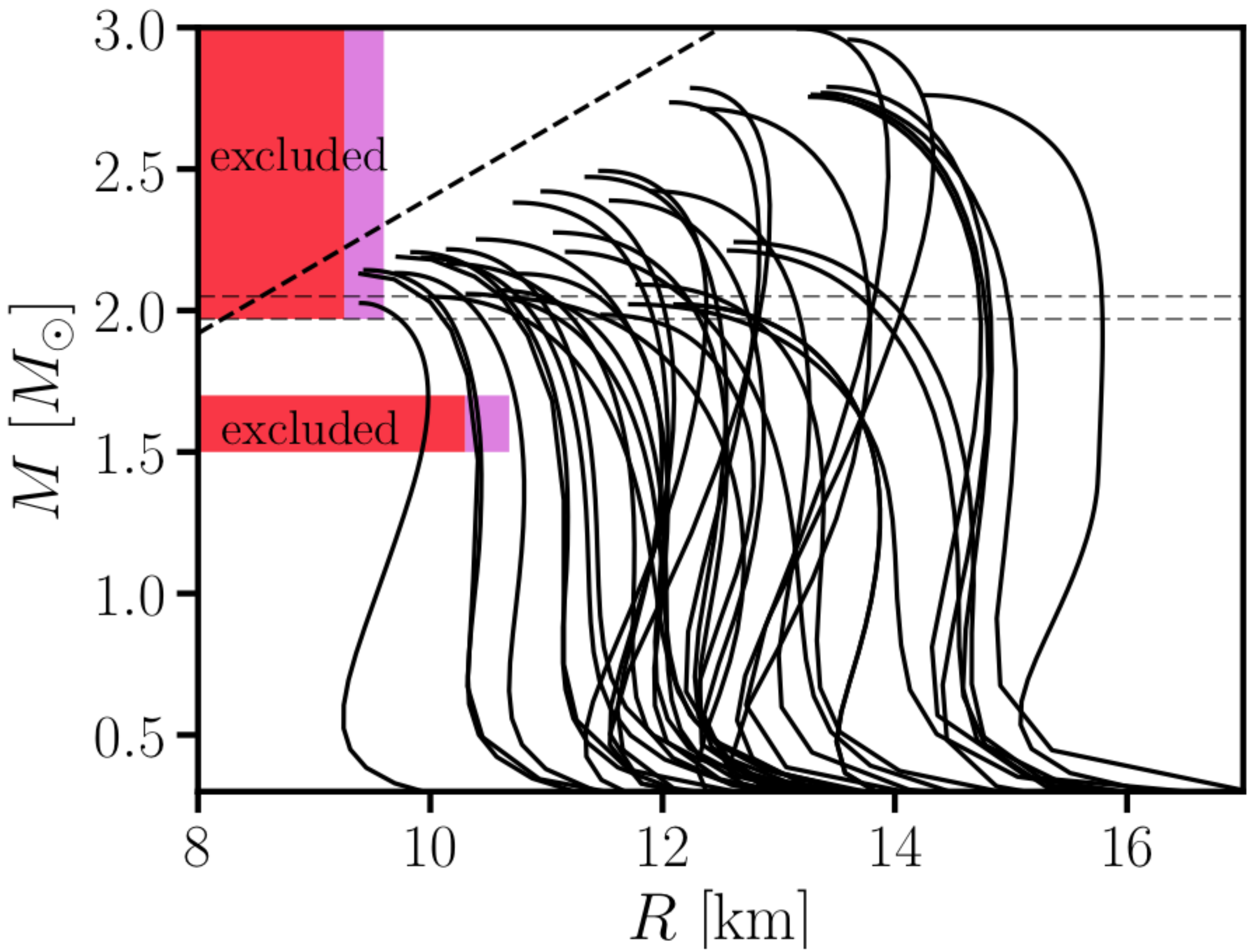

FIRST RADIUS CONSTRAINTS FROM GW's

Bauswein, Just, Janka, NS - ApJ Letters (2017)

Assume that each EOS is *maximally compact* above the density for 1.5 M_{sun} and combine with $M_{thres} > 2.74\ M_{sun}$

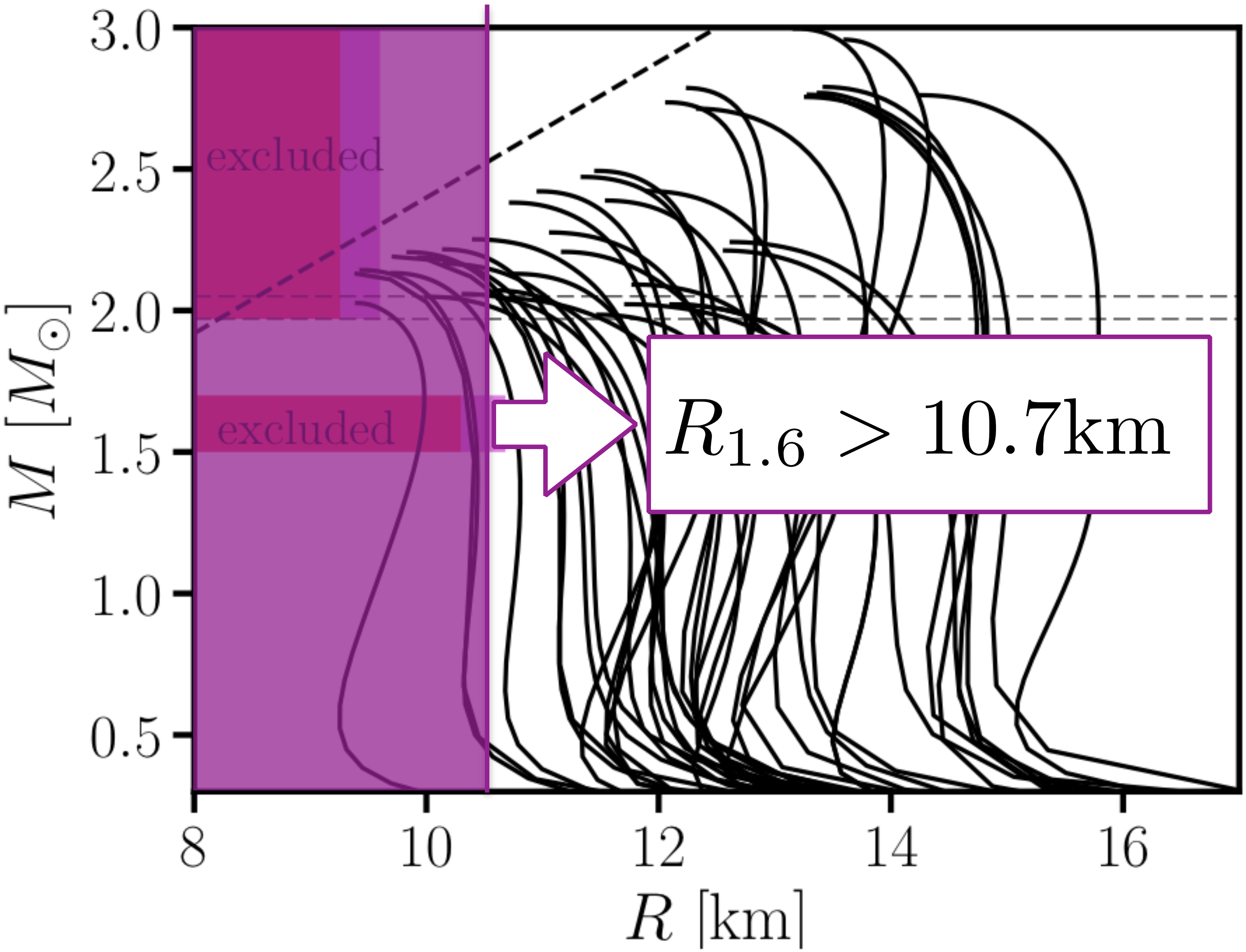

CONSTRAINTS FROM FUTURE DETECTIONS

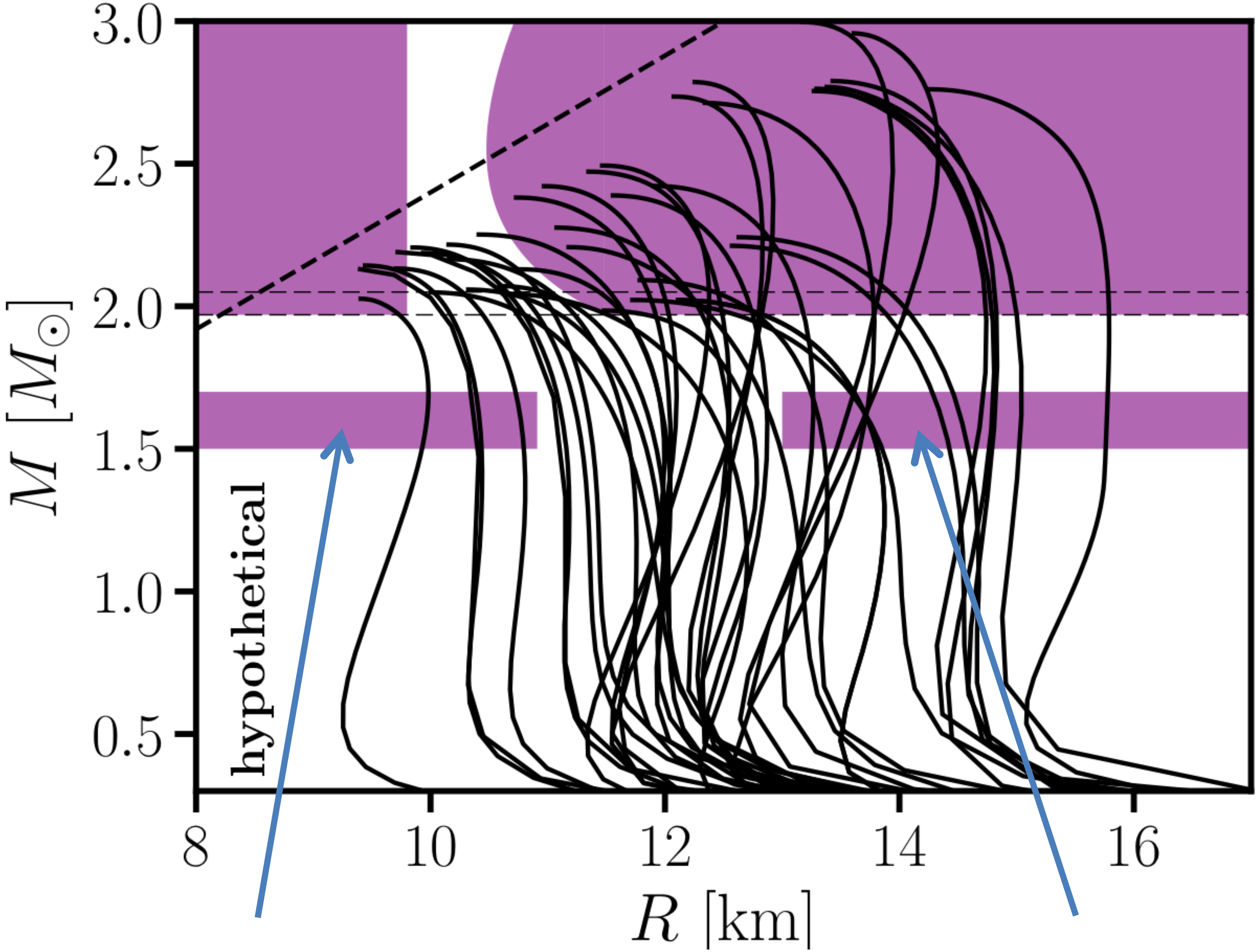

No collapse with
M=2.9Msun

Collapse with
M=3.1Msun

Post-Merger Gravitational Waves

The GW signal can be divided into three distinct phases: *inspiral*, *merger* and *post-merger ringdown*.

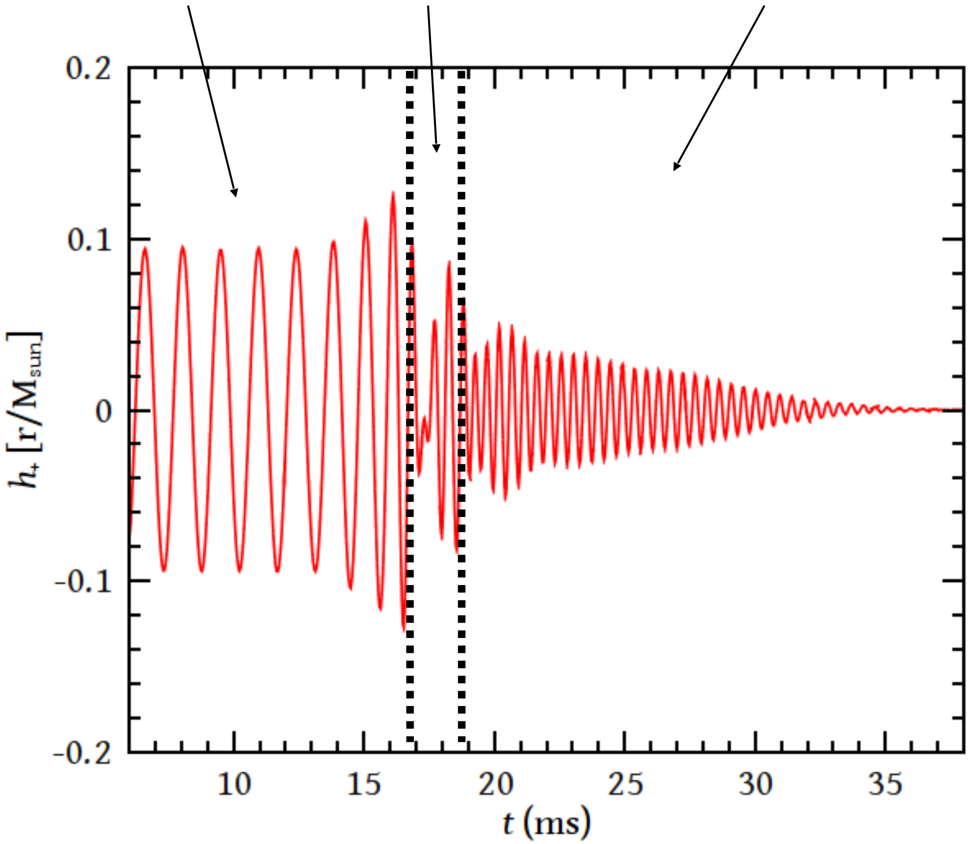

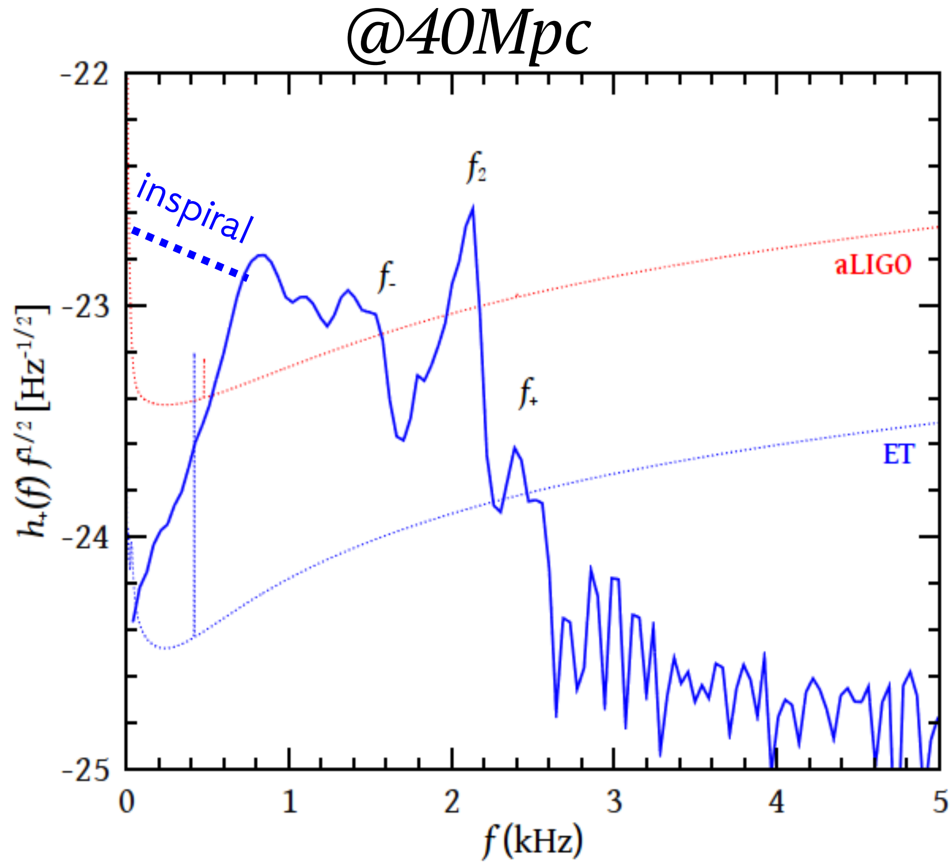

Several peaks stand above the aLIGO/VIRGO or ET sensitivity curves and are potentially detectable. Are these *oscillations* of the HMNS?

Spacetime Evolution

90´s Nakamura, Oohara, Kojima / Shibata, Nakamura / Baumgarte, Shapiro

Definitions

$$\tilde{\gamma}_{ij} = e^{-4\phi}\gamma_{ij}$$

$$e^{4\phi} = \gamma^{1/3} \equiv \det(\gamma_{ij})^{1/3}$$

$$\tilde{A}_{ij} = e^{-4\phi}A_{ij} \quad A_{ij} = K_{ij} - \frac{1}{3}\gamma_{ij}K,$$

$$\tilde{\Gamma}^i := \tilde{\gamma}^{jk}\tilde{\Gamma}^i_{jk} = -\tilde{\gamma}^{ij}{}_{,j}$$

"1+log" lapse function

$$\partial_t \alpha = -2\alpha A$$

$$\partial_t A = \partial_t K$$

"Gamma-driver" shift condition

$$\partial_t \beta^i = B^i$$

$$\partial_t B^i = \frac{3}{4}\alpha\partial_t\tilde{\Gamma}^i - e^{-4\phi}\beta^i$$

Time evolution

$$\frac{d}{dt}\tilde{\gamma}_{ij} = -2\alpha\tilde{A}_{ij}, \qquad \frac{d}{dt} = \partial_t - \mathcal{L}_\beta$$

$$\frac{d}{dt}\phi = -\frac{1}{6}\alpha K.$$

$$\frac{d}{dt}K = -\gamma^{ij}D_iD_j\alpha + \alpha\left[\tilde{A}_{ij}\tilde{A}^{ij} + \frac{1}{3}K^2 + \frac{1}{2}(\rho + S)\right],$$

$$\frac{d}{dt}\tilde{A}_{ij} = e^{-4\phi}[-D_iD_j\alpha + \alpha(R_{ij} - S_{ij})]^{TF}$$

$$+\alpha(K\tilde{A}_{ij} - 2\tilde{A}_{il}\tilde{A}^l_j),$$

$$\frac{\partial}{\partial t}\tilde{\Gamma}^i = -2\tilde{A}^{ij}\alpha_{,j} + 2\alpha\left(\tilde{\Gamma}^i_{jk}\tilde{A}^{kj} - \frac{2}{3}\tilde{\gamma}^{ij}K_{,j} - \tilde{\gamma}^{ij}S_j + 6\tilde{A}^{ij}\phi_{,j}\right)$$

$$-\frac{\partial}{\partial x^j}\left(\beta^l\tilde{\gamma}^{ij}{}_{,l} - 2\tilde{\gamma}^{m(j}\beta^{i)}_{,m} + \frac{2}{3}\tilde{\gamma}^{ij}\beta^l_{,l}\right).$$

einsteintoolkit.org

Open Source code for 3D simulations in General Relativity
C/C++/Fortran90 with MPI+OpenMP

einstein toolkit

Home About Download Documentation Help! Contribute Gallery

The Einstein Toolkit

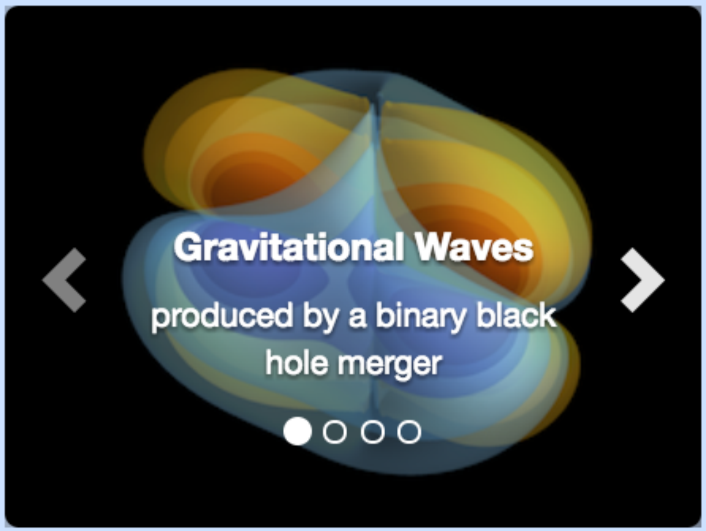

Gallery

20+ years of development
(started as private version)

About

The Einstein Toolkit is a community-driven software platform of core computational tools to advance and support research in relativistic astrophysics and gravitational physics.

About

Documentation

A lot of the documentation within the Einstein Toolkit is generated from comments in the source code, and more can be found on the Einstein Toolkit Wiki or other documents. We provide links to guides, tutorials and references.

Documentation

Download

We provide a convenient method to get all of the Einstein Toolkit with just a few commands, and explain the whole process.

Download Try it now!

Contribute

The Einstein Toolkit would not exist without numerious contributions from its community. It is easy to learn how you can contribute as well.

Contribute

Gallery of Examples

einstein toolkit

Home About Download Documentation Help! Contribute **Gallery**

Einstein Toolkit Gallery

This page contains example simulations that can be run using the Einstein Toolkit, either exclusively or in combination with external codes. The parameter files and thornlists required to reproduce the simulations are provided. Some examples also include images and movies, analysis and visualisation scripts, example simulation data, and tutorials.

Binary black hole GW150914

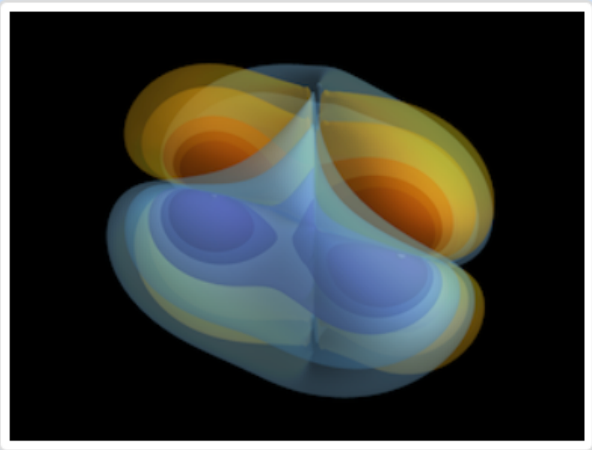

Poisson equation

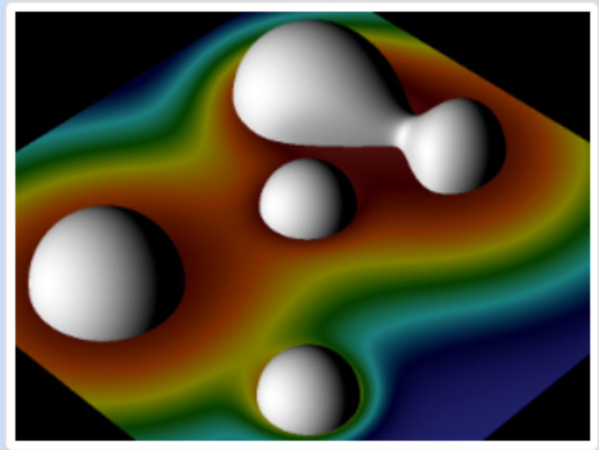

Multi Patch Energy Equation

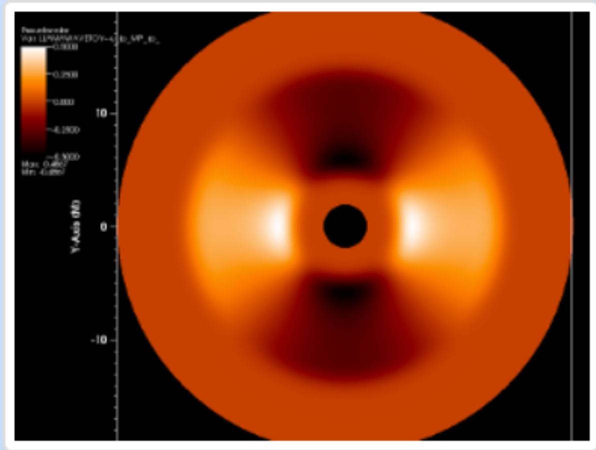

Single, stable neutron star

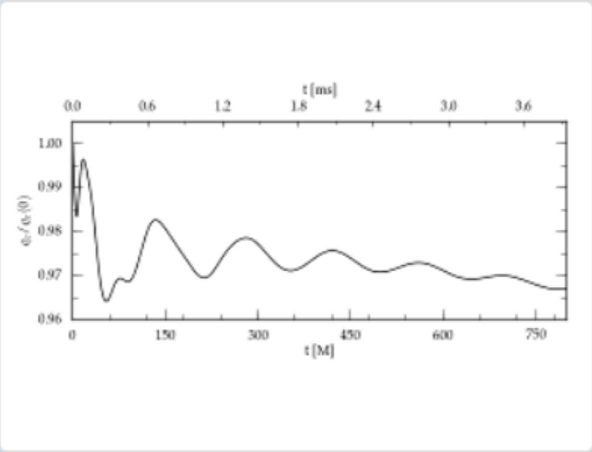

Binary neutron star

Gallery of Examples

einstein toolkit

Home | About | Download | Documentation | Help! | Contribute | **Gallery**

Einstein Toolkit Gallery

This page contains example simulations that can be run using the Einstein Toolkit, either exclusively or in combination with external codes. The parameter files and thornlists required to reproduce the simulations are provided. Some examples also include images and movies, analysis and visualisation scripts, example simulation data, and tutorials.

Binary black hole GW150914

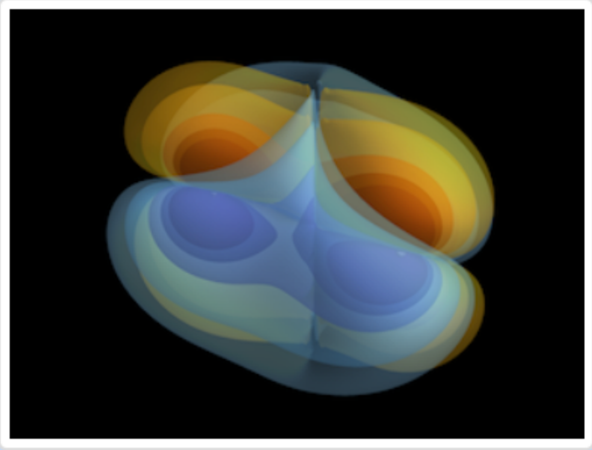

Poisson equation

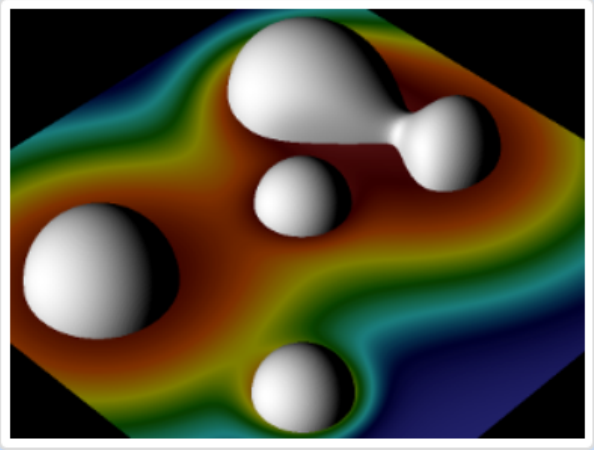

Multi Patch Energy Equation

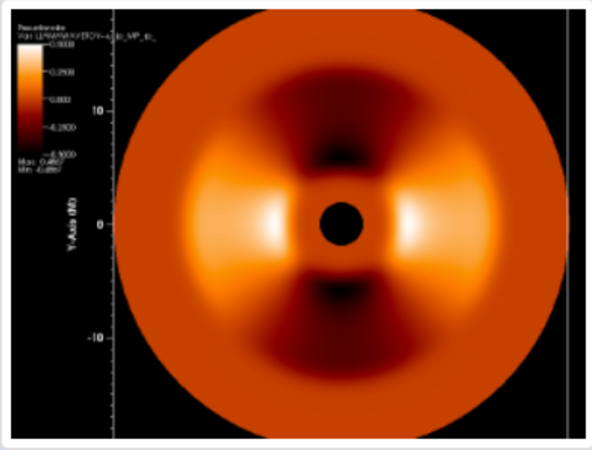

Single, stable neutron star

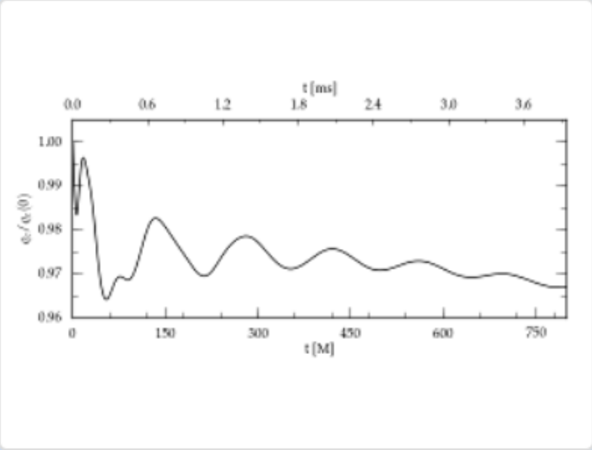

Binary neutron star

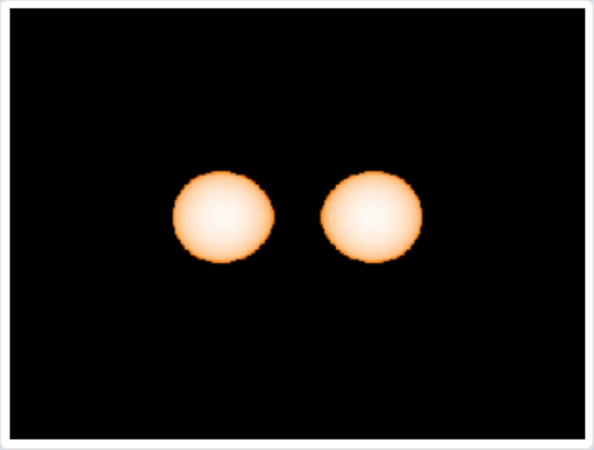

RNSID: Initial Data for Rotating Neutron Stars

(developed at AUTH)

Adaptive Mesh Refinement

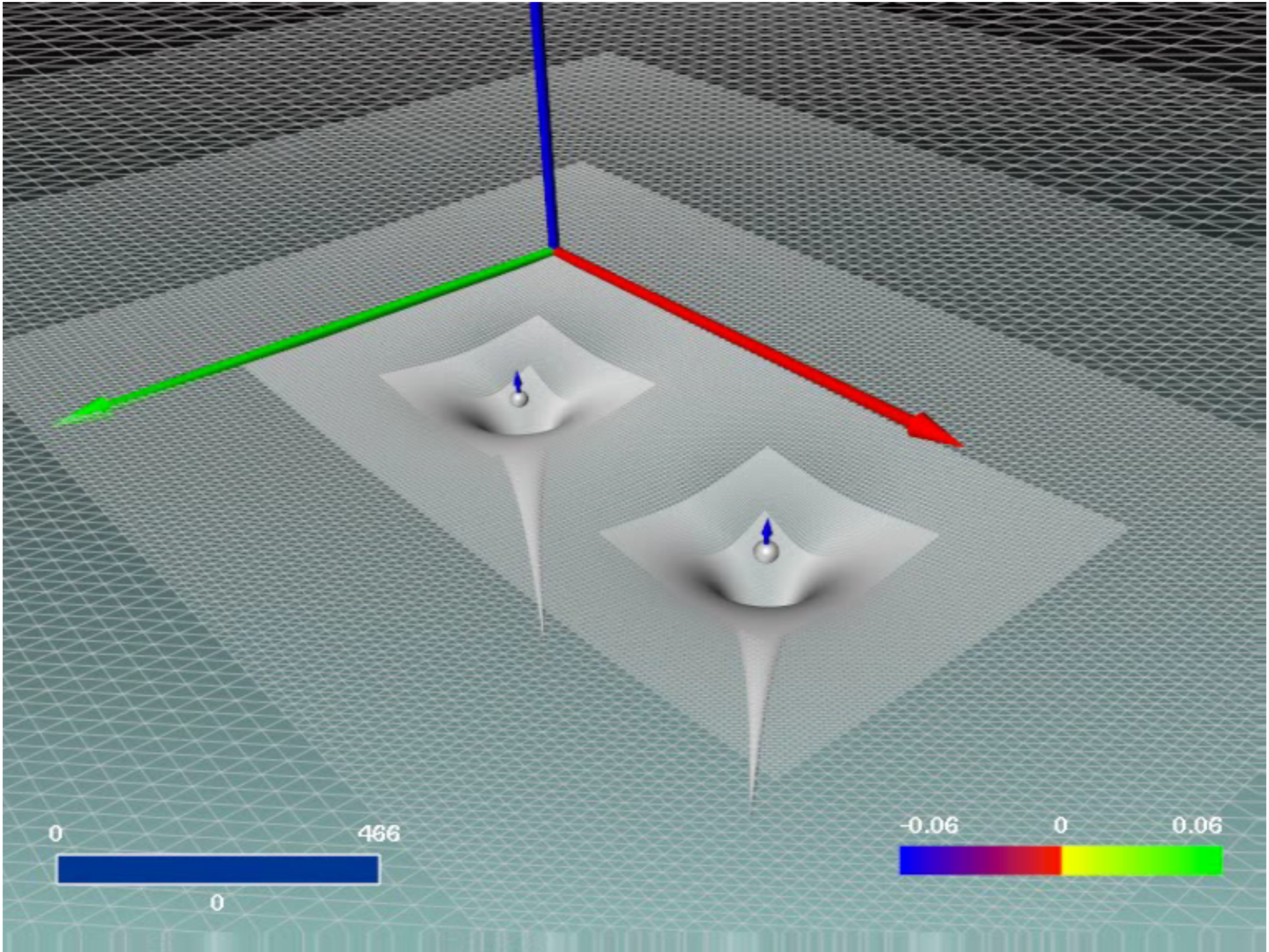

ARIS (ΕΔΕΤ - Athens)

426 IBM cpu's = 8500 cores
1000 TB space



BNS Merger on ARIS

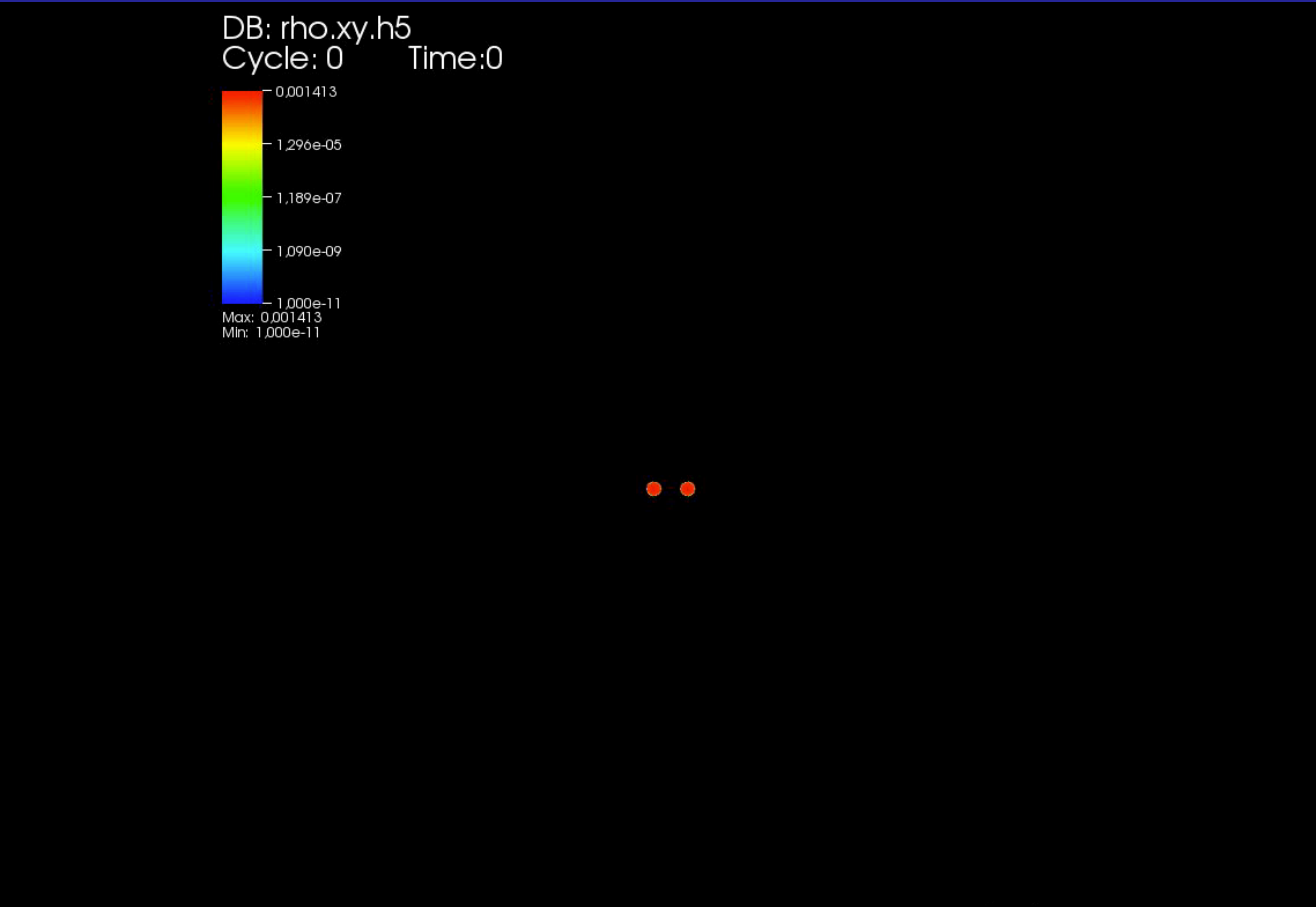

Running on ARIS

2016 (pr002022) 900.000 CPU hours

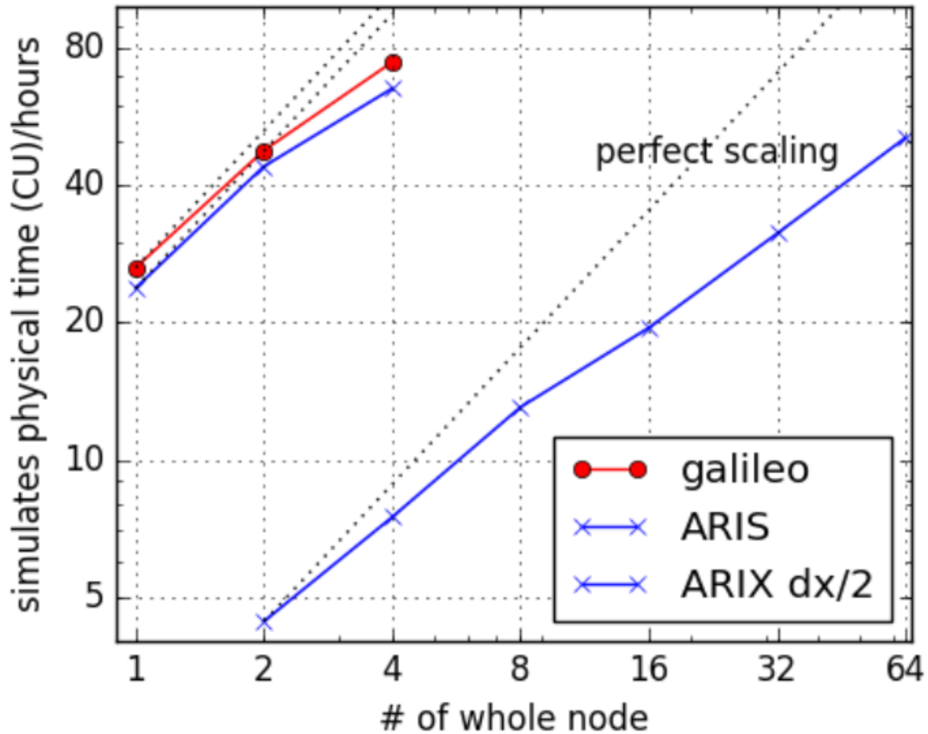

2017 (pr004019) 900.000 CPU hours

Run type	# Runs	# Steps/Run	Walltime (seconds)/Step	# CPU cores	Total core hours/Type Run
Merger Δx = 0.185 (360,360,100) 6 levels	12	90000	4.6	320	73000

Post-Merger GW Oscillations

GRAVITATIONAL WAVES

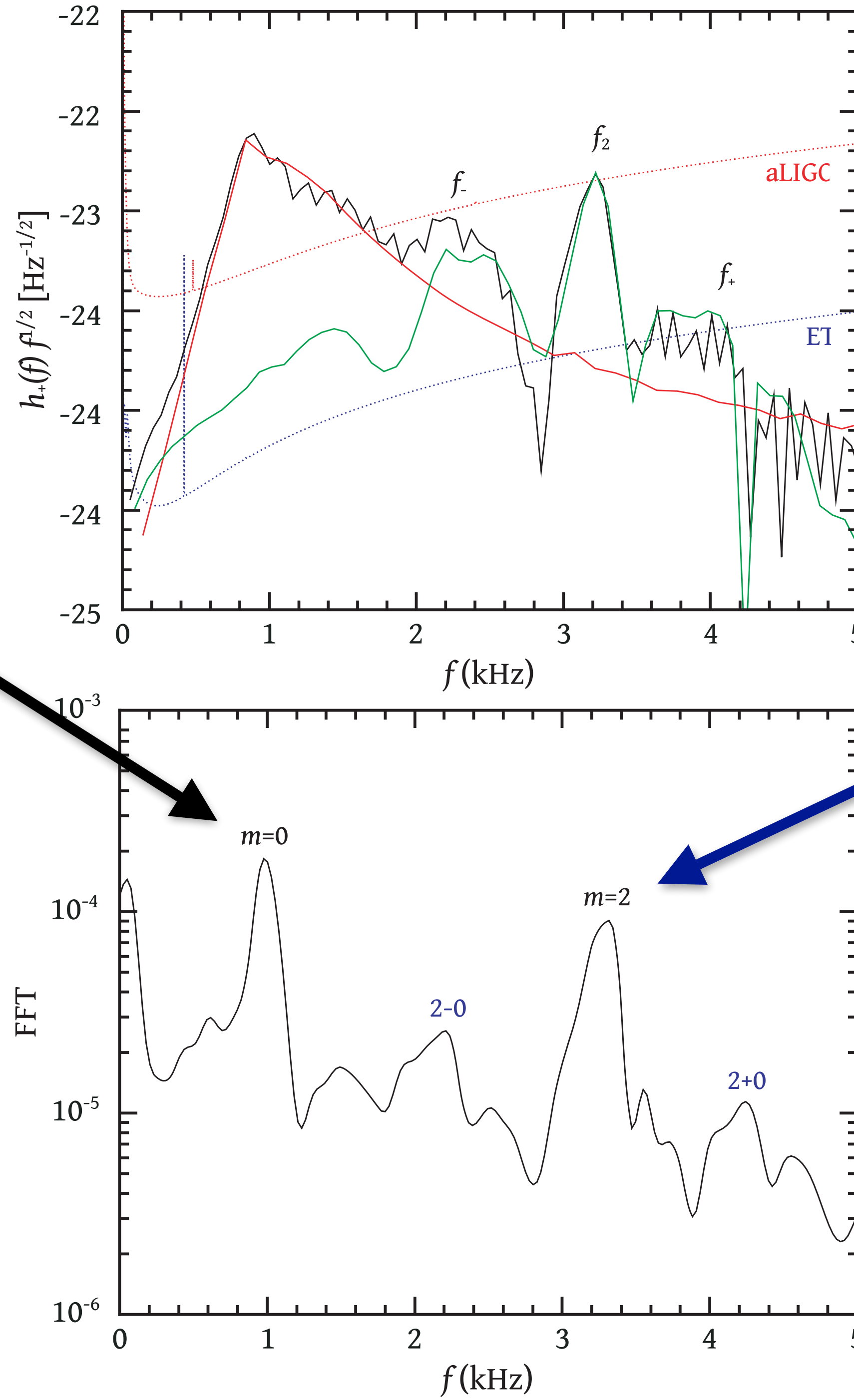

m=0 radial mode

HYDRODYNAMICS

m=2 quadrupole mode

Post-Merger GW Oscillations

GRAVITATIONAL WAVES

HYDRODYNAMICS

m=0 radial mode

m=2 quadrupole mode

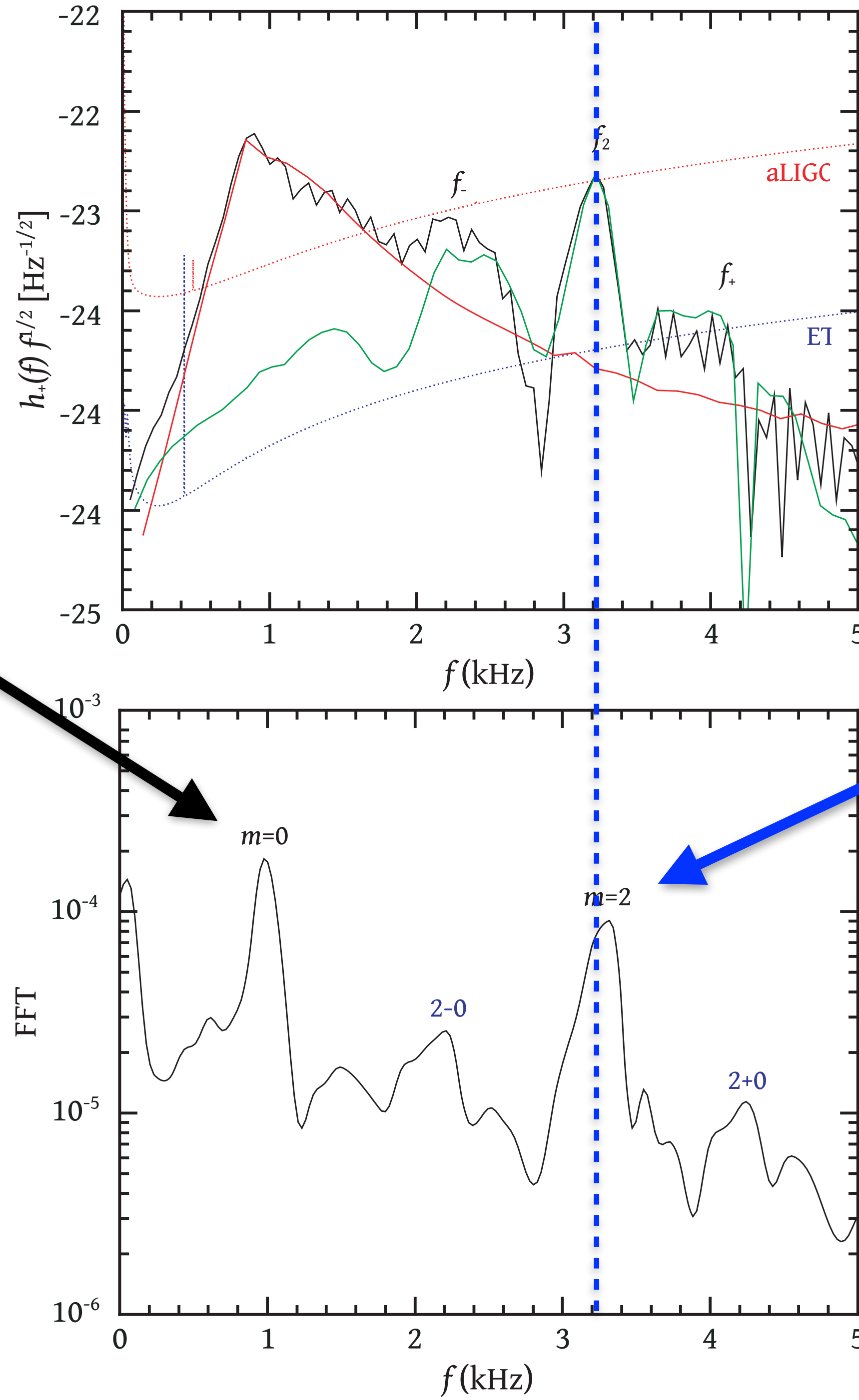

Post-Merger GW Oscillations

GRAVITATIONAL WAVES

HYDRODYNAMICS

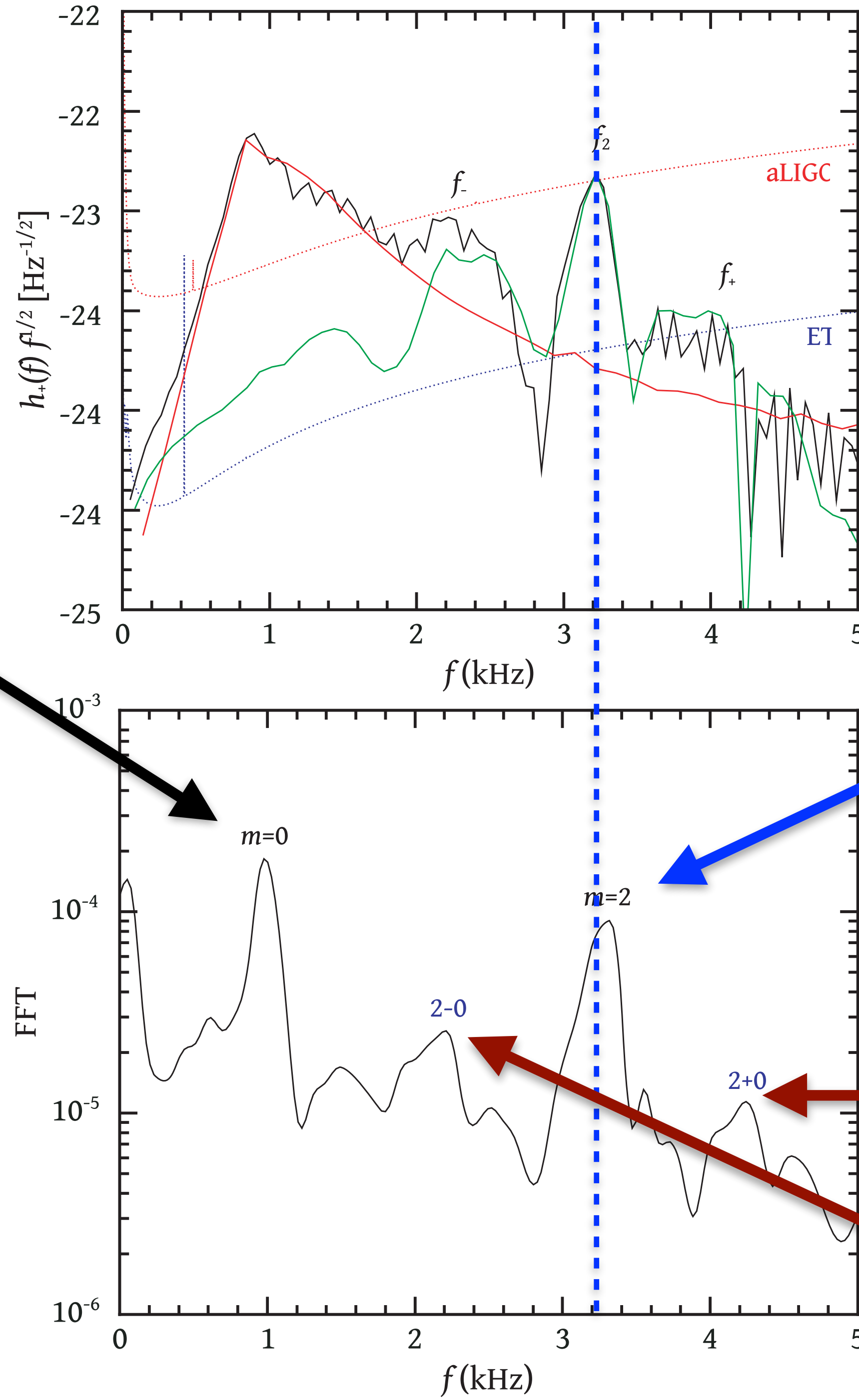

m=0 radial mode

m=2 quadrupole mode

“2-0” and “2+0” quasi-linear combination frequency

Post-Merger GW Oscillations

GRAVITATIONAL WAVES

HYDRODYNAMICS

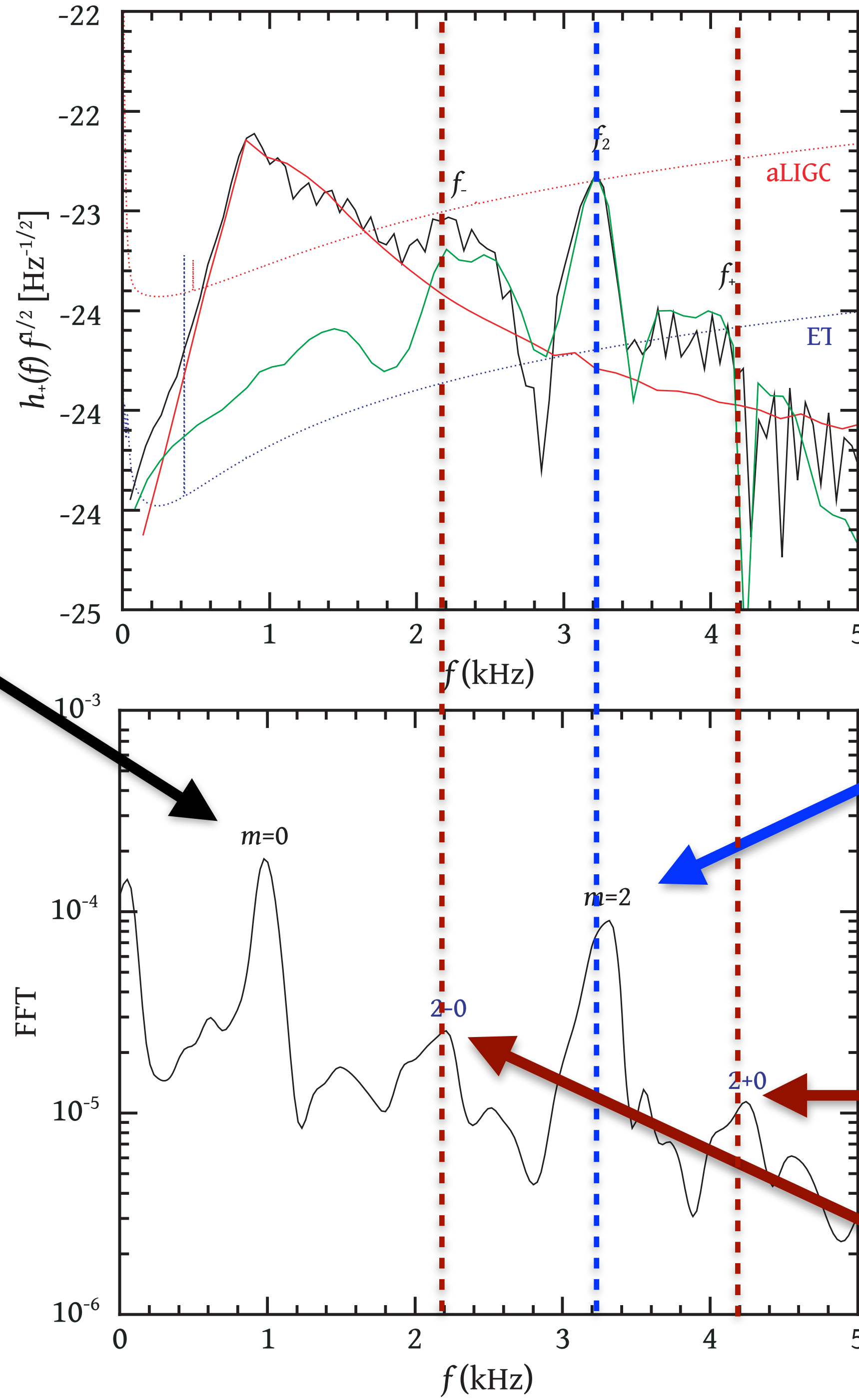

m=0 radial mode

m=2 quadrupole mode

"2-0" and "2+0" quasi-linear combination frequency

Nonradial Oscillations

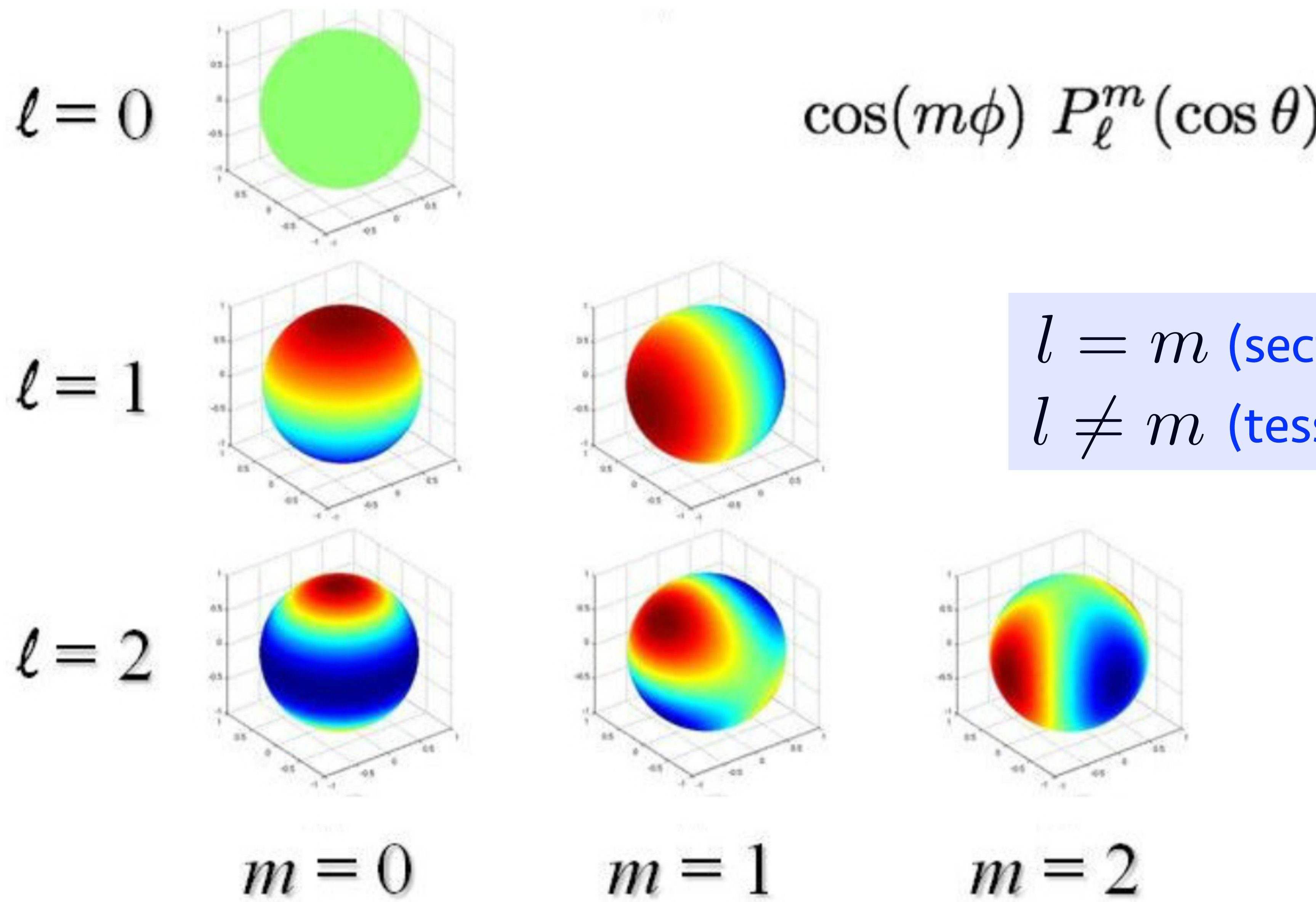

$l = m$ (sectoral)

$l \neq m$ (tesseral)

(zonal)

Nonradial Oscillations of Neutron Stars

Main oscillation modes:

1. *f*-modes / *p*-modes

   fluid modes restored by pressure

2. *g*-modes

   restored by gravity/buoyancy in non-isentropic stars

3. inertial modes (*r*-modes)

   restored by the Coriolis force in rotating stars

4. *w*-modes

   spacetime modes (similar to black hole modes)

GW-detection: *f*-, *p*-, *g*-, *r*-modes : stable oscillations

instabilities

Quadrupole Frequencies for Nonrotating Stars

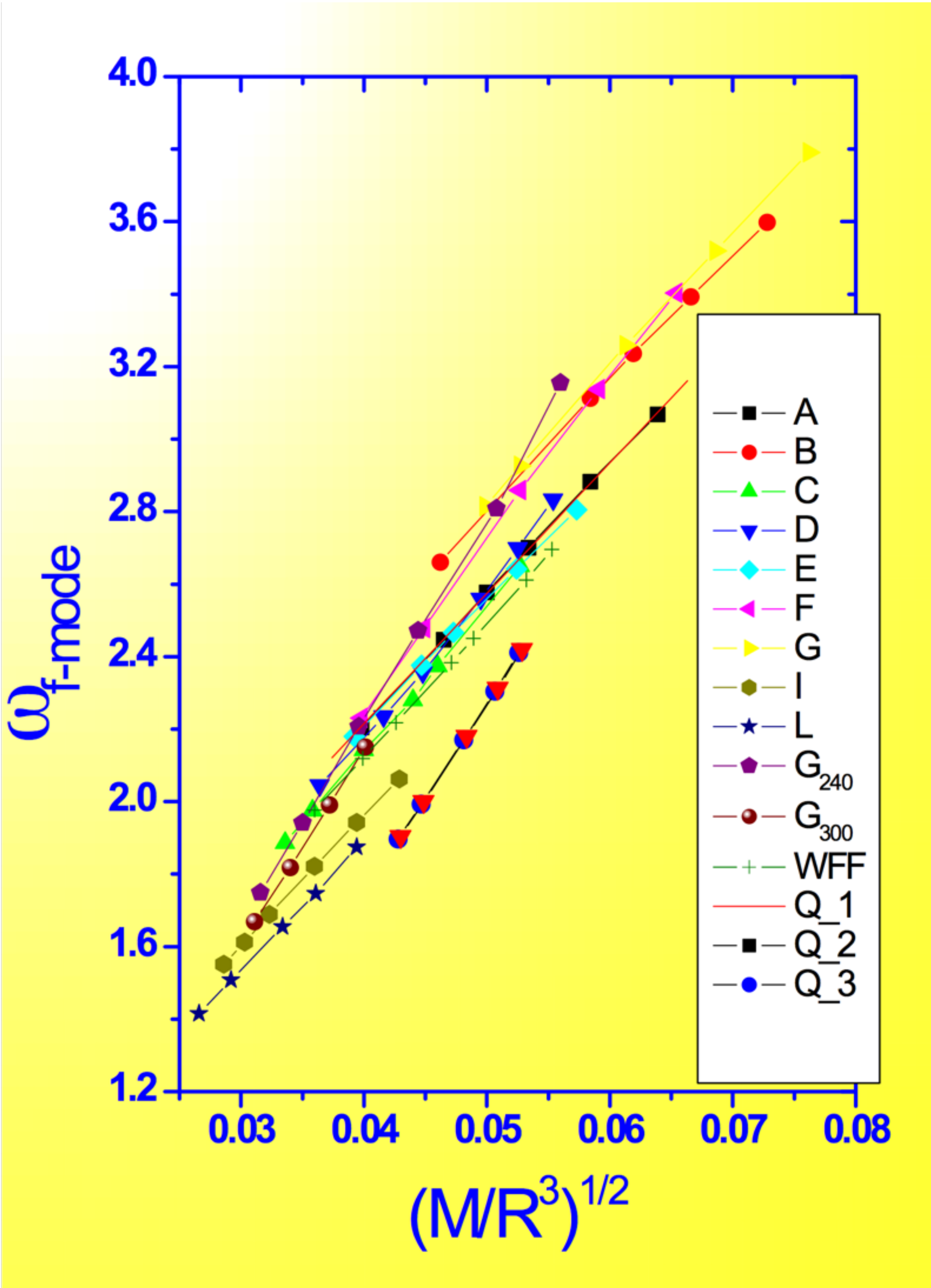

Empirical relations for GW asteroseismology:

$$\omega_f\,(kHz) \approx 0.78 + 1.637\left(\frac{M_{1.4}}{R_{10}^{\ 3}}\right)^{1/2}$$

Andersson & Kokkotas (1998)

Spiral Deformation

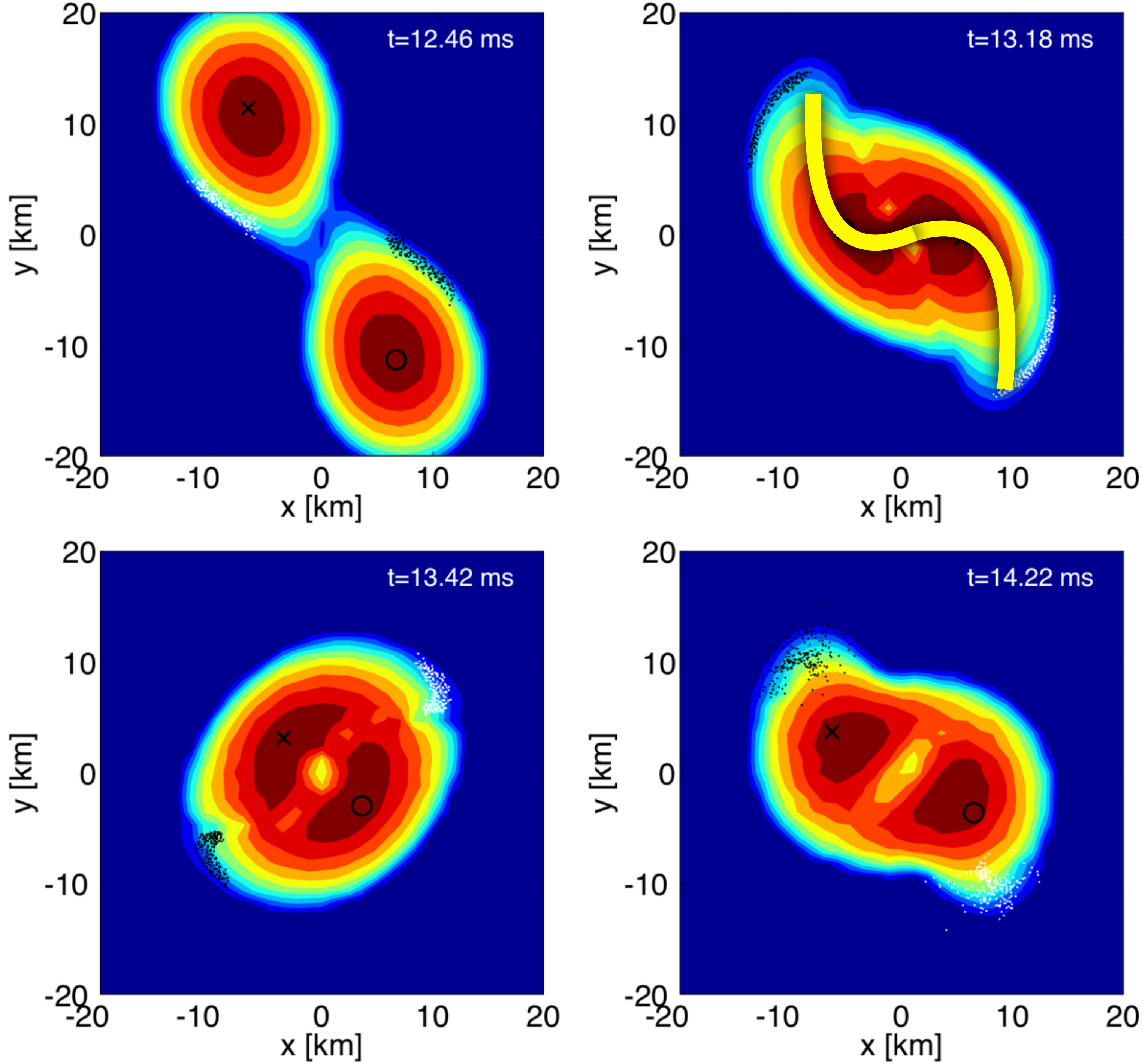

Bauswein & NS (2015)

Post-Merger GW Oscillations

Bauswein, NS (2015)

GRAVITATIONAL WAVE SPECTRUM

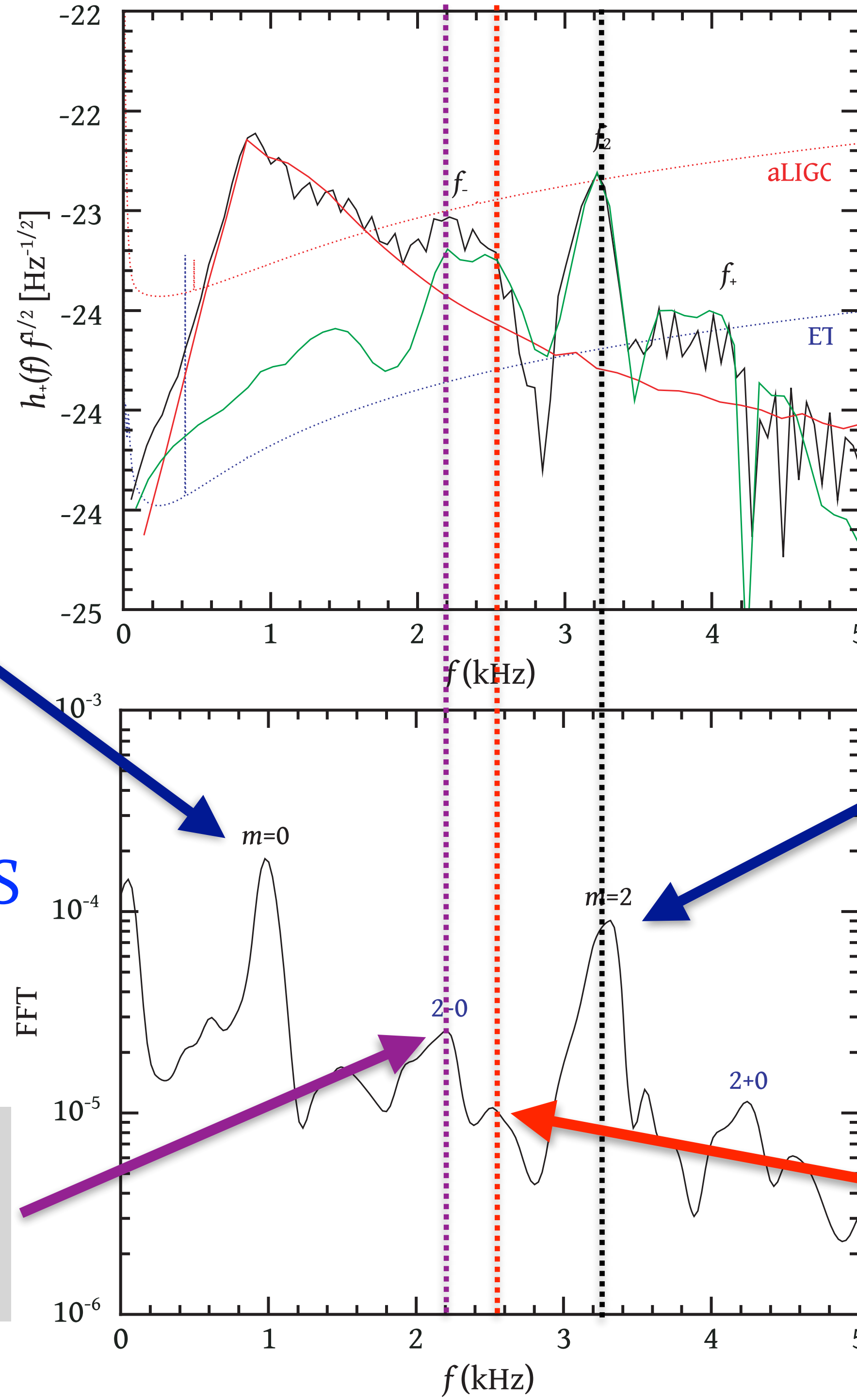

l=m=0
linear quasi-radial mode

FFT OF HYDRODYNAMICS IN EQUATORIAL PLANE

l=m=2
linear f-mode

"2-0" quasi-linear
combination frequency

nonlinear
spiral frequency

linear + quasi-linear + nonlinear

Bauswein, NS (2015)

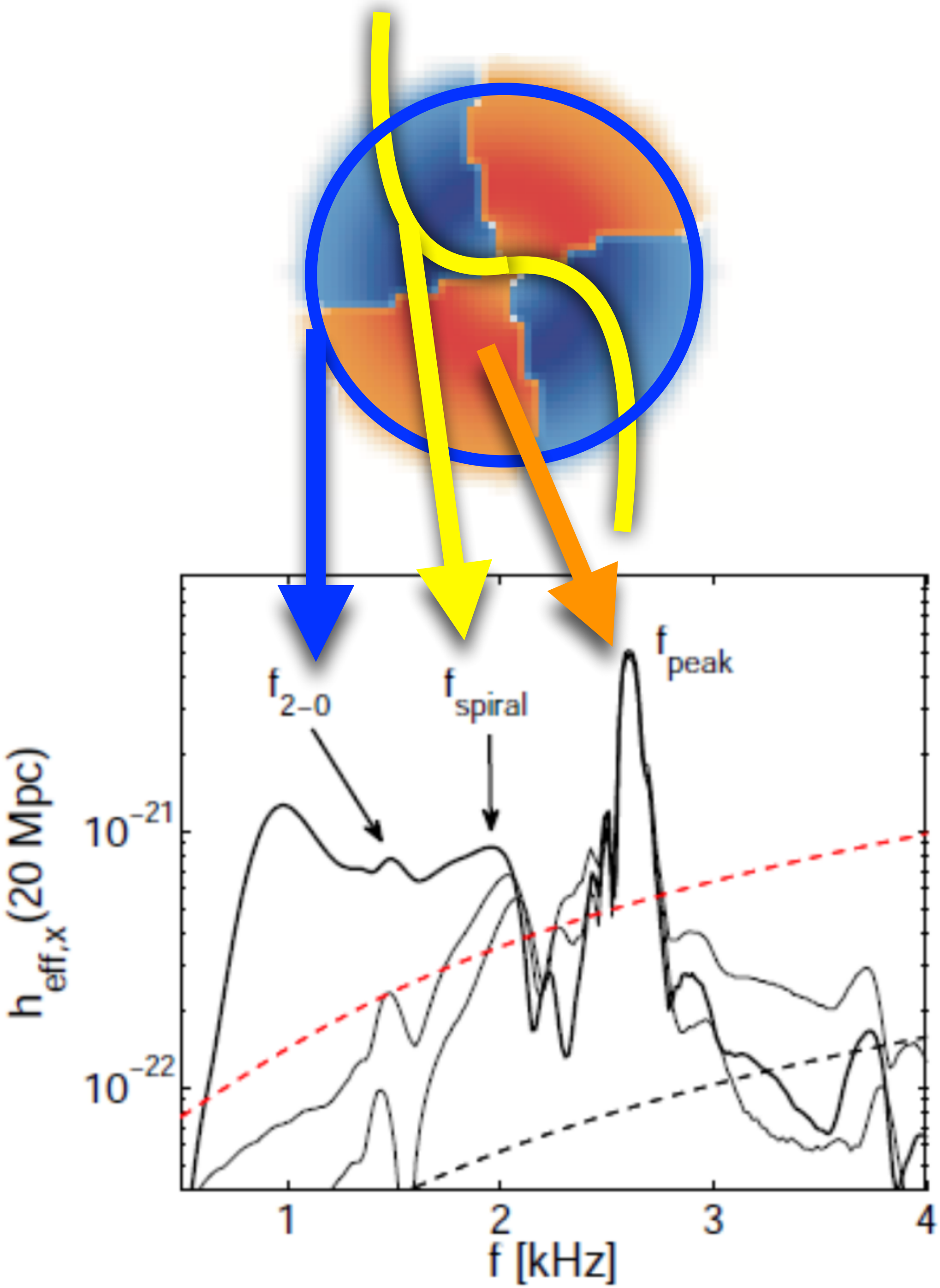

Three Types of Post-Merger Dynamics

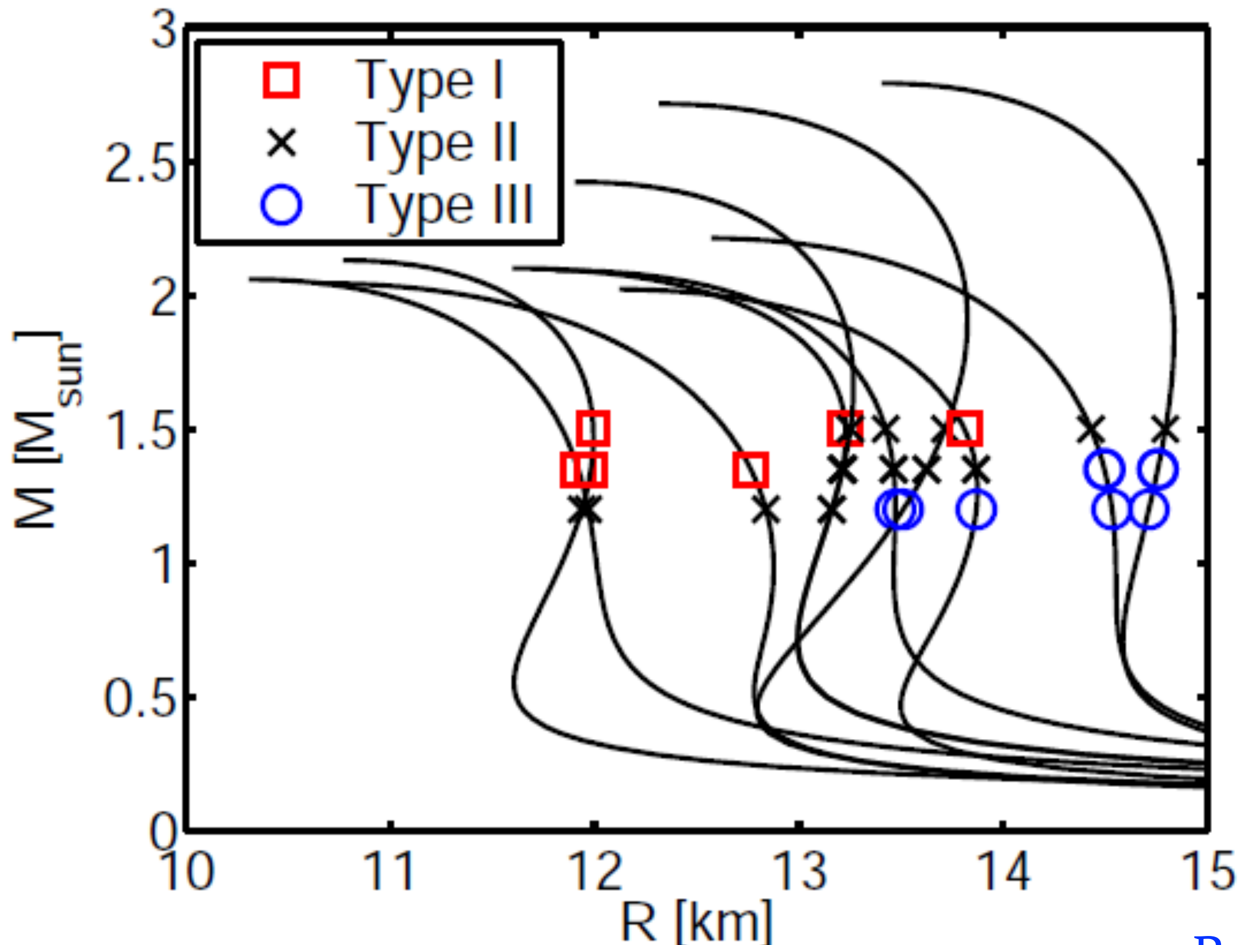

Bauswein, NS (2015)

Type I: the "2-0" combination frequency dominates

Type II: **both** the "2-0" and the f_{spiral} frequencies are present

Type III: the f_{spiral} frequency dominates

Radius Determination from Post-Merger Signal

Bauswein, Janka, Hebeler & Schwenk (2012)

f_{peak} correlates very well with the radius @ 1.6 Msun, if M_{tot} is known from inspiral.

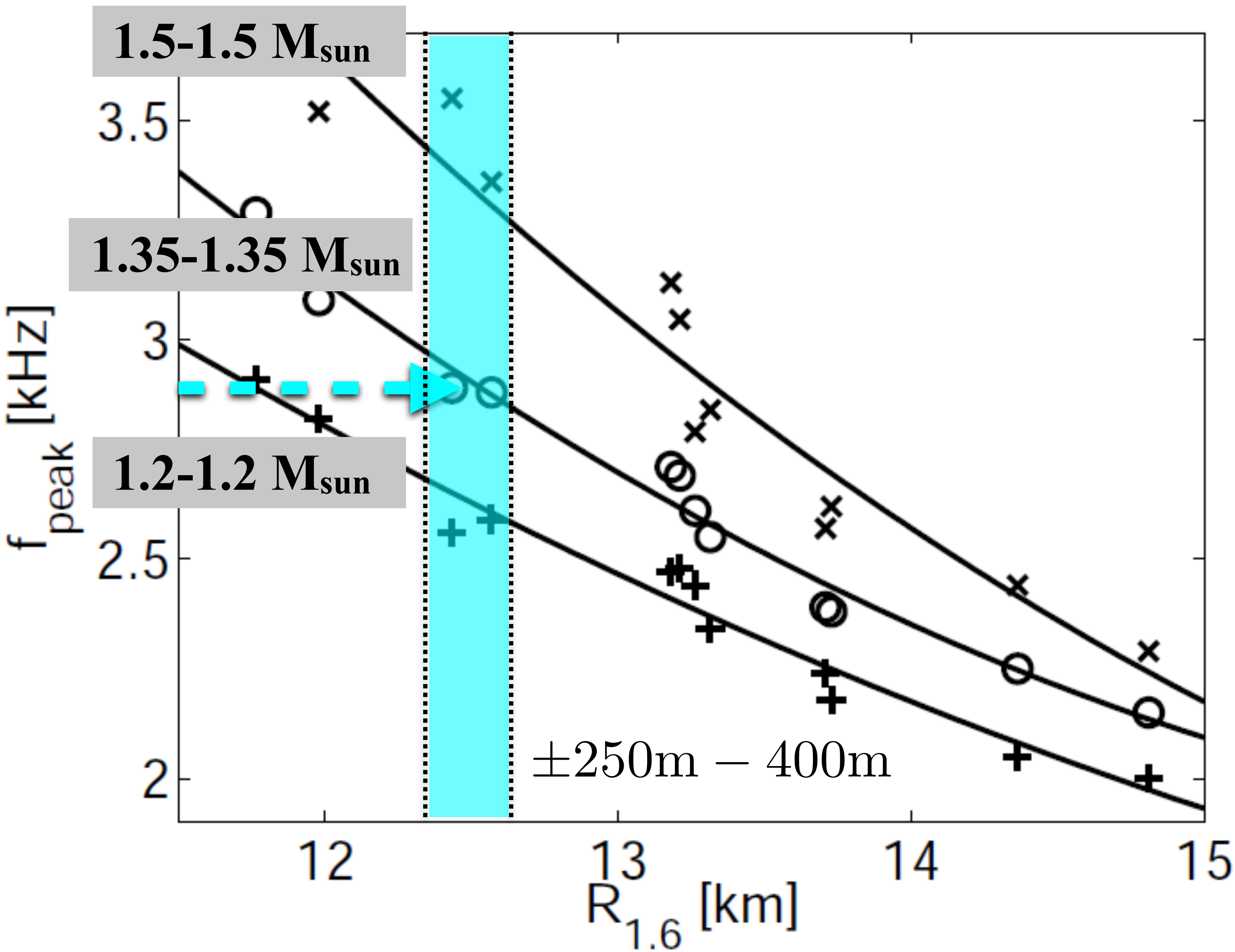

Breaking the EOS Degeneracy

Bauswein, NS, Janka (2014)

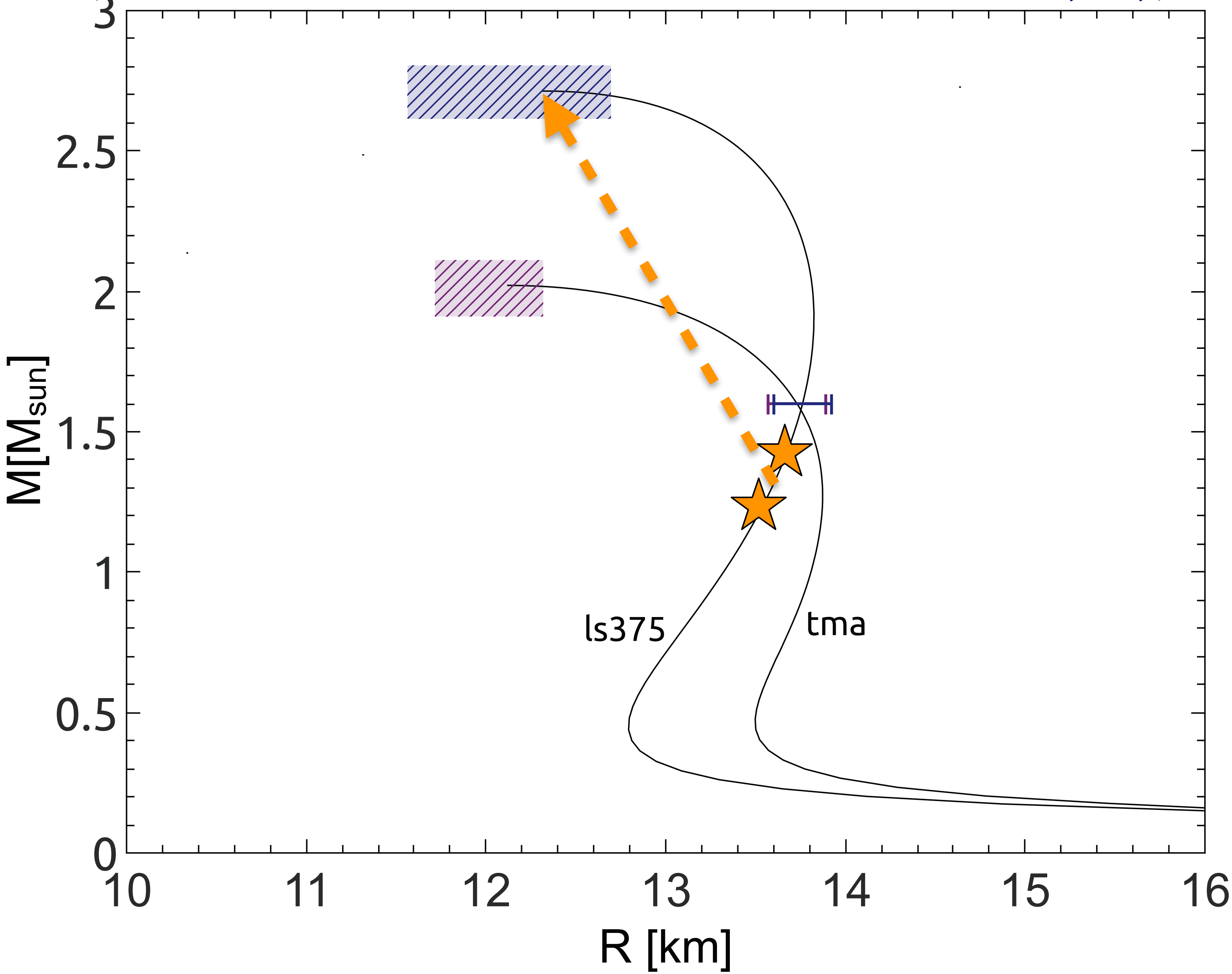

Principal Component Analysis (PCA)

Clark, Bauswein, NS, Shoemaker (2016)

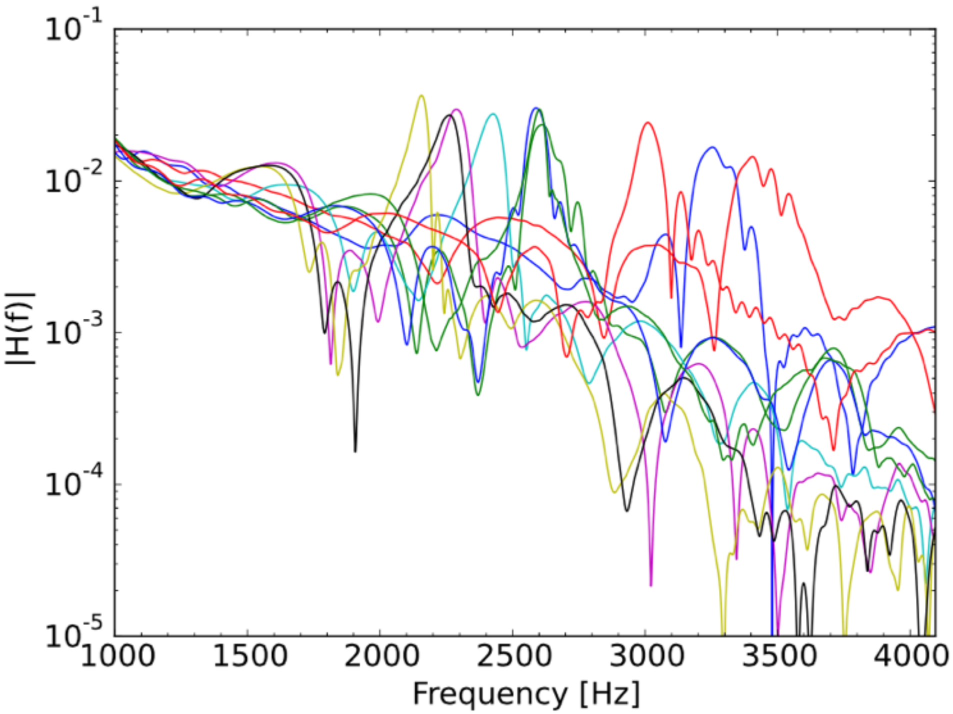

Actual fft's for different models.

Principal Component Analysis (PCA)

Clark, Bauswein, NS, Shoemaker (2016)

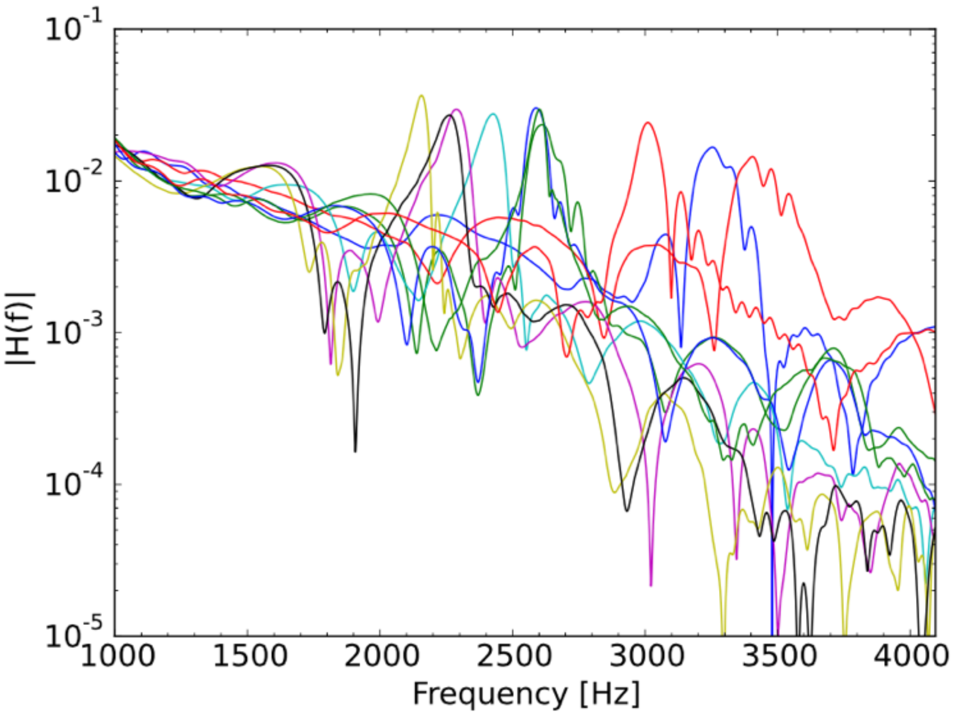

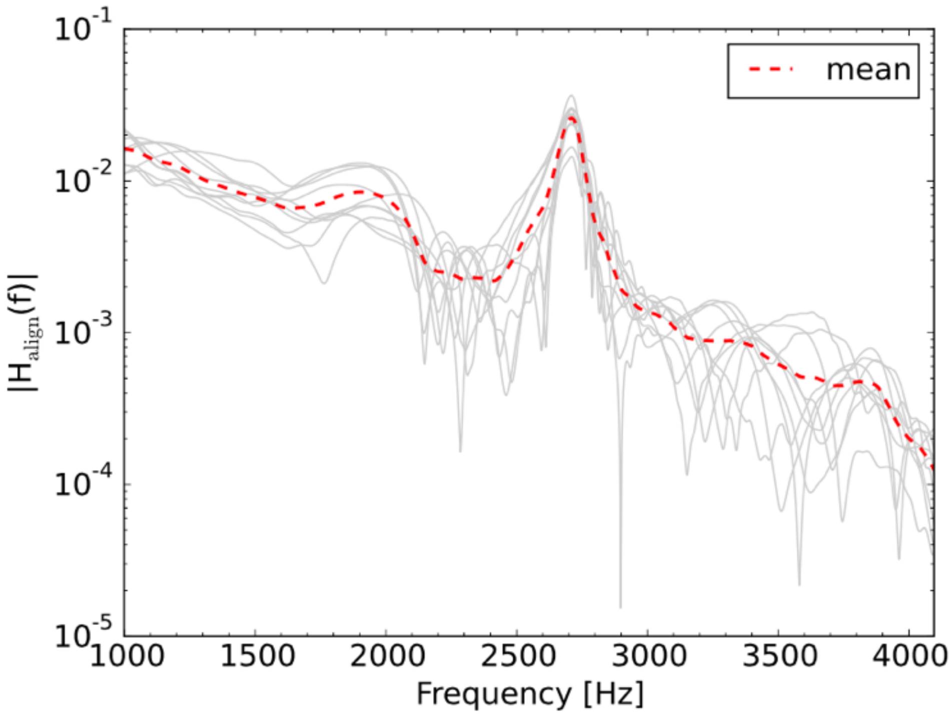

Actual fft's for different models.

Rescaled to common reference model.

Principal Component Analysis (PCA)

Clark, Bauswein, NS, Shoemaker (2016)

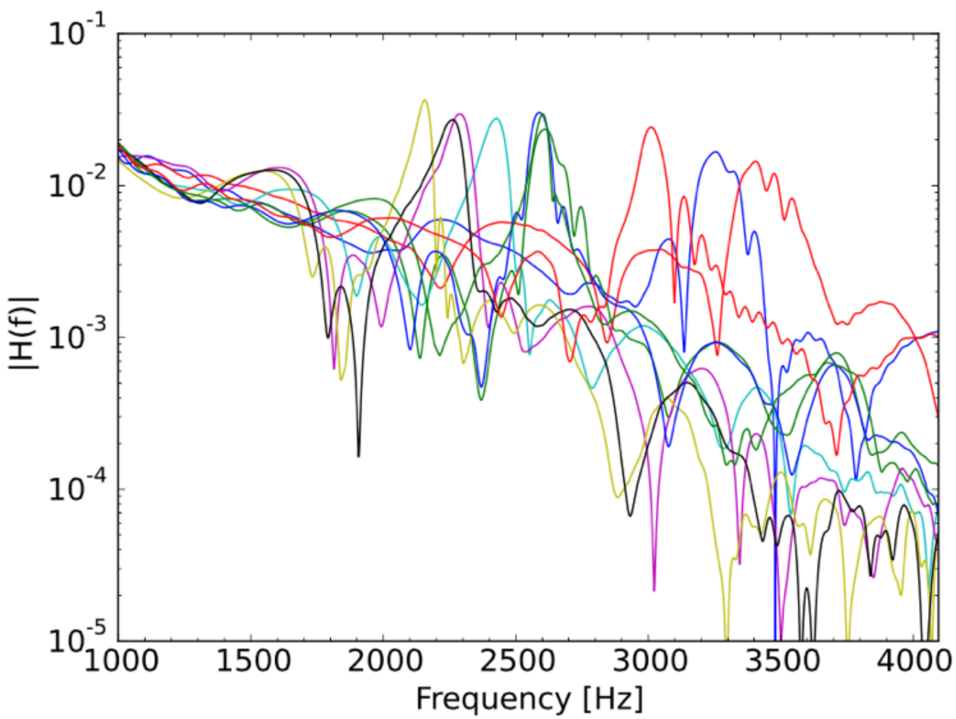

Actual fft's for different models.

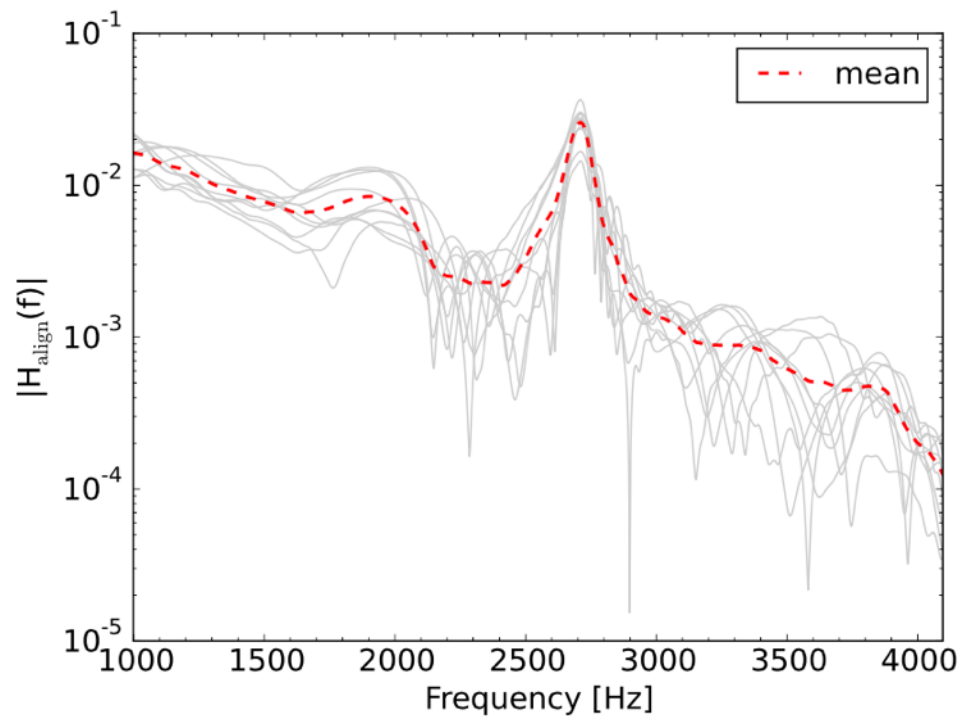

Rescaled to common reference model.

Our PCA template extracts >90% of signal power compared to only 40% when using simple burst analysis.

Detectability

Clark, Bauswein, NS, Shoemaker (2016)

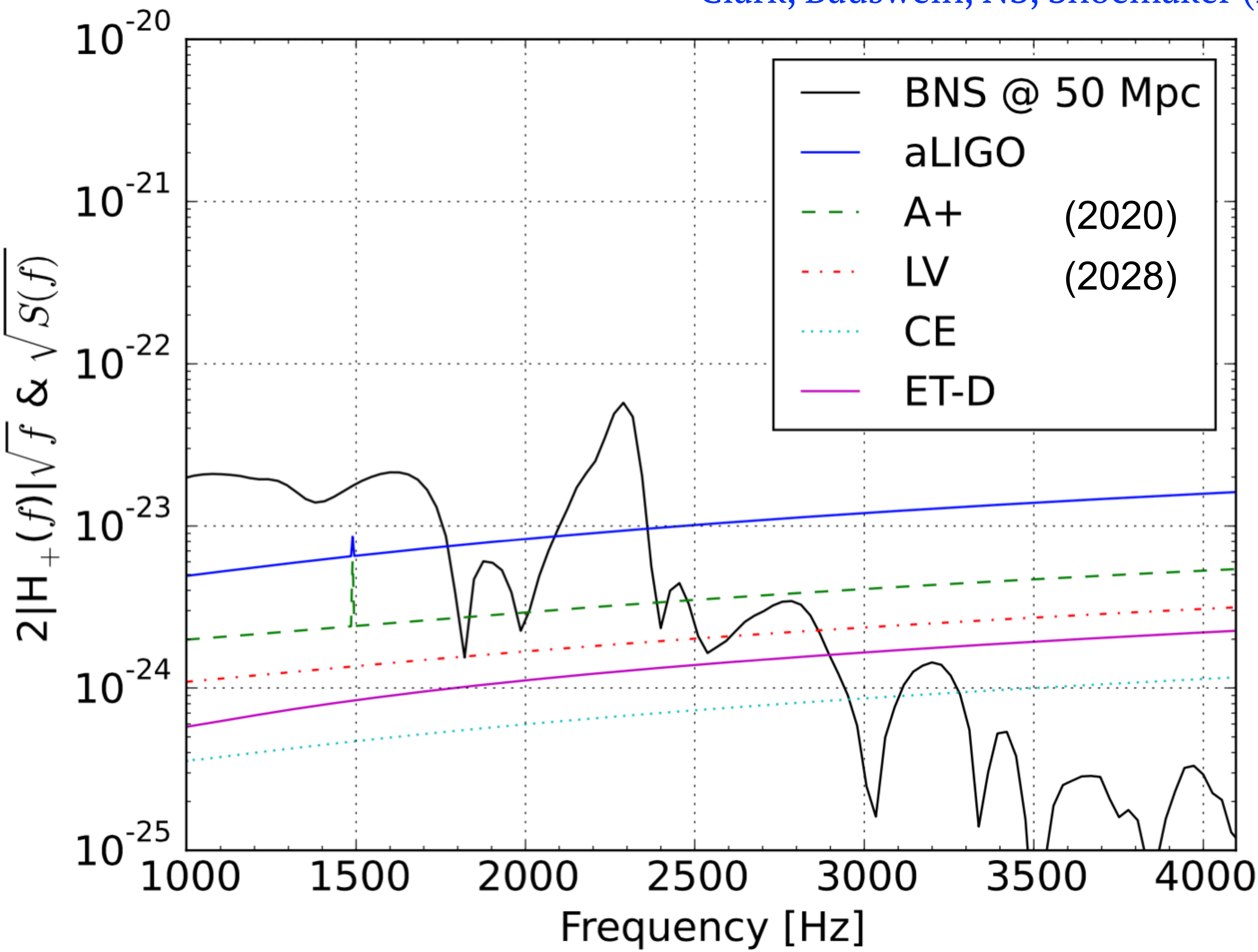

Coherent Wave Burst Analysis

Clark, Bauswein, NS, Shoemaker (2016)

Instrument	$\mathrm{SNR}_{\mathrm{full}}$	$\mathrm{SNR}_{\mathrm{post}}$	D_{hor} [Mpc]	$\dot{\mathcal{N}}_{\mathrm{det}}$ [year^{-1}]
aLIGO	$2.99_{2.37}^{3.86}$	$1.48_{1.13}^{1.86}$	$29.89_{23.76}^{38.57}$	$0.01_{0.01}^{0.03}$
A+	$7.89_{6.25}^{10.16}$	$4.19_{3.26}^{5.35}$	$78.89_{62.52}^{101.67}$	$0.13_{0.10}^{0.20}$
LV	$14.06_{11.16}^{18.13}$	$7.28_{5.64}^{9.30}$	$140.56_{111.60}^{181.29}$	$0.41_{0.21}^{0.88}$
ET-D	$26.65_{20.81}^{34.28}$	$12.16_{9.34}^{15.31}$	$266.52_{208.06}^{342.80}$	$2.81_{1.33}^{5.98}$
CE	$41.50_{32.99}^{53.52}$	$20.52_{15.72}^{25.83}$	$414.62_{329.88}^{535.221}$	$10.59_{5.33}^{22.78}$

PLANNED UPGRADES AND NEW DETECTORS

Clark, Bauswein, NS, Shoemaker (2016)

LIGO A+ [74, 75] a set of upgrades to the existing LIGO facilities, including frequency-dependent squeezed light, improved mirror coatings and potentially increased laser beam sizes. Noise amplitude spectral sensitivity would be improved by a factor of $\sim$ 2.5-3 over 1–4 kHz. A+ could begin operation as early as 2017–18.

LIGO Voyager (LV) [75] a major upgrade to the existing LIGO facilities, including higher laser power, changes to materials used for suspensions and mirror substrates and, possibly, low temperature operation. LV would become operational around 2027–28 and offer noise amplitude spectral sensitivity improvements of $\sim$ 4.5-5 over 1–4 kHz.

LIGO Cosmic Explorer (CE) [75] a new LIGO facility rather than an upgrade, with operation envisioned to commence after 2035, probably as part of a network with LIGO Voyager. In its simplest incarnation, Cosmic Explorer would be a straightforward extrapolation of A+ technology to a much longer arm length of 40 km, referred to as CE1 which would be $\sim 14\times$ more sensitive than aLIGO over 1–4 kHz. An alternative extrapolation is that of Voyager technology to the 40 km arm length, referred to as CE2. CE2 is only $\sim 8\times$ more sensitive than aLIGO for the frequency range of interest in this study. For simplicity, we consider only CE1.

Einstein Telescope (ET-D) [76, 77] the European third-generation GW detector. In this work, we consider the ET-D configuration which is comprised of two individual inteferometers where one targets low frequency sensitivity and the other high frequency sensitivity. Both interferometers will be of 10 km arm length and housed in an underground facility. Furthermore, the full observatory will consist of three such detectors in a triangle arrangement. ET-D is $\sim 8\times$ more sensitive than aLIGO over 1–4 kHz. Due to the network configuration (i.e., the alignment of the component instruments) the effective sensitivity of ET-D is $\sim$ 18% higher than that for a single ET-D detector.

Inertial Modes!

(submitted to PRL, 2017)

Convective excitation of inertial modes in binary neutron star mergers

Roberto De Pietri,[1,2] Alessandra Feo,[3,2] José A. Font,[4,5] Frank Löffler,[6,7]
Francesco Maione,[1,2] Michele Pasquali,[1,2] and Nikolaos Stergioulas[8]

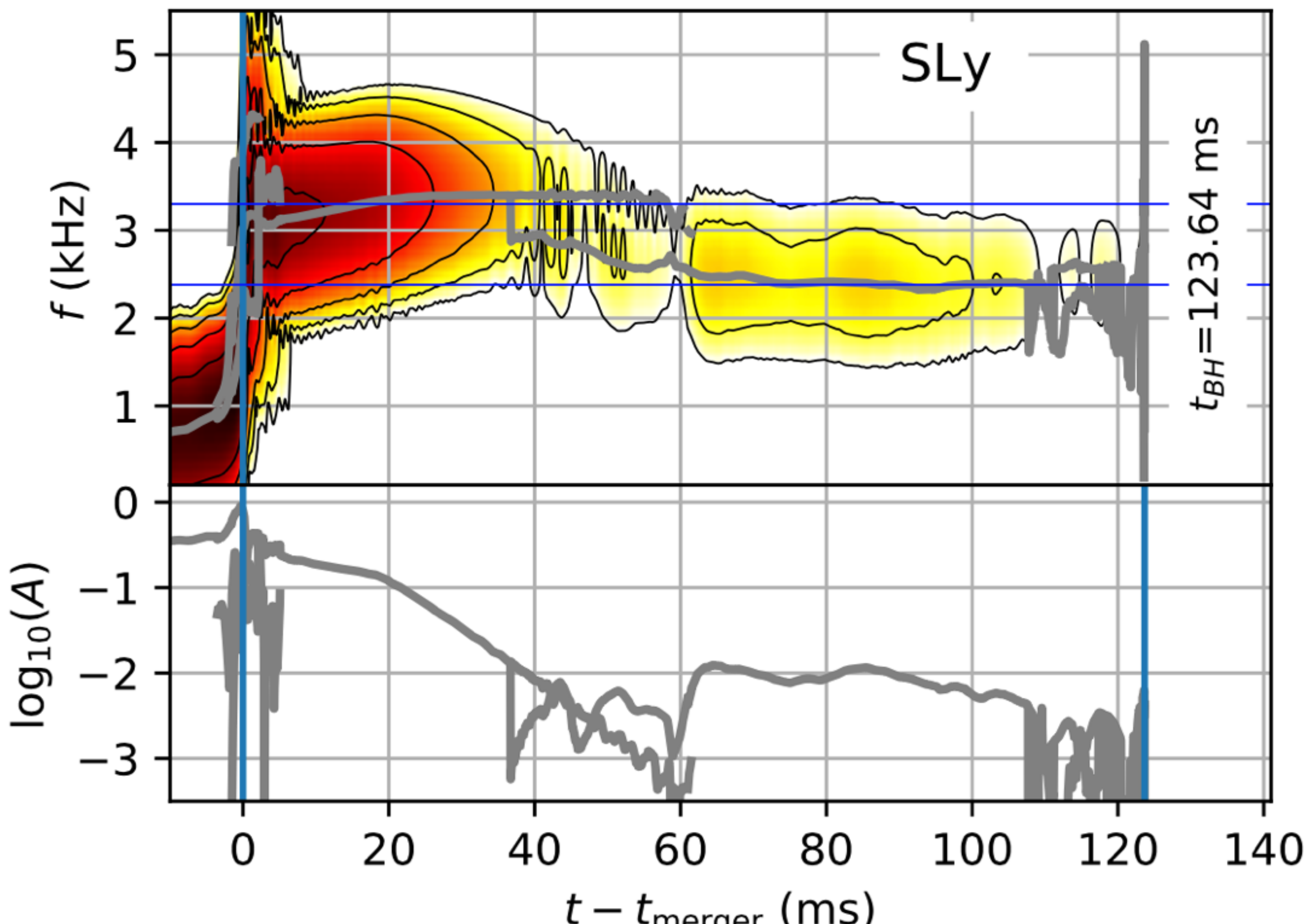

30 million core hours (PRACE)

Convective Instability

The local convective instability depends on the sign of the Schwarzschild discriminant

$$A_\alpha = \frac{1}{\varepsilon + p}\nabla_\alpha \varepsilon - \frac{1}{\Gamma_1 p}\nabla_\alpha p.$$

where

$$\Gamma_1 := (\varepsilon + p)/p(dp/d\varepsilon)_s = (d\ln p/d\ln \rho)_s$$

is the adiabatic index.

$A_\alpha < 0$ convective stability

$A_\alpha > 0$ convective instability

For a piecewise-polytropic EOS with a thermal component, we find analytically:

$$\Gamma_1 = \Gamma_{\rm th} + (\Gamma_i - \Gamma_{\rm th})\frac{K_i \rho^{\Gamma_i}}{p}.$$

Convective Instability

The sign of A_r in the equatorial plane:

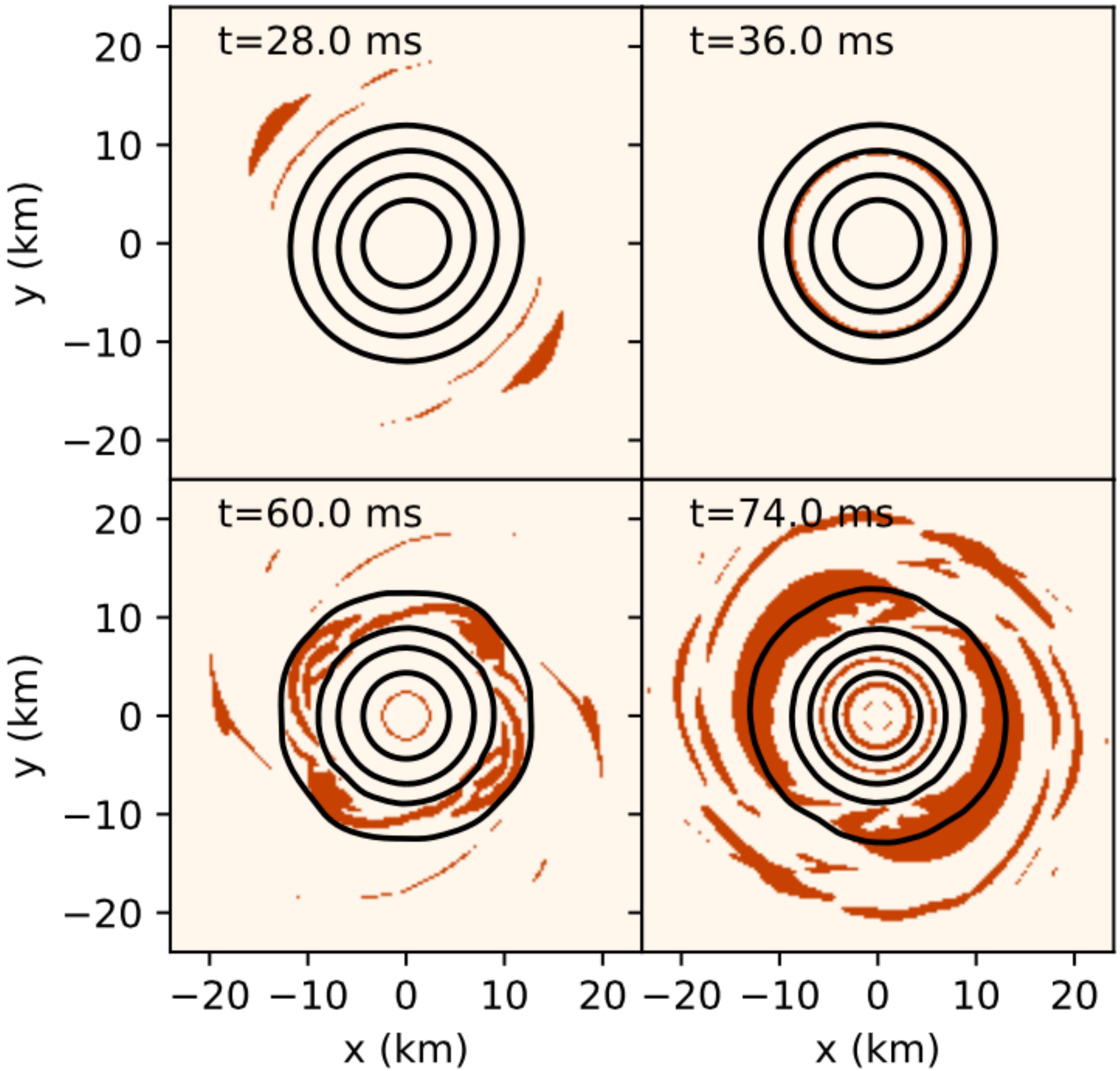

Convective Instability

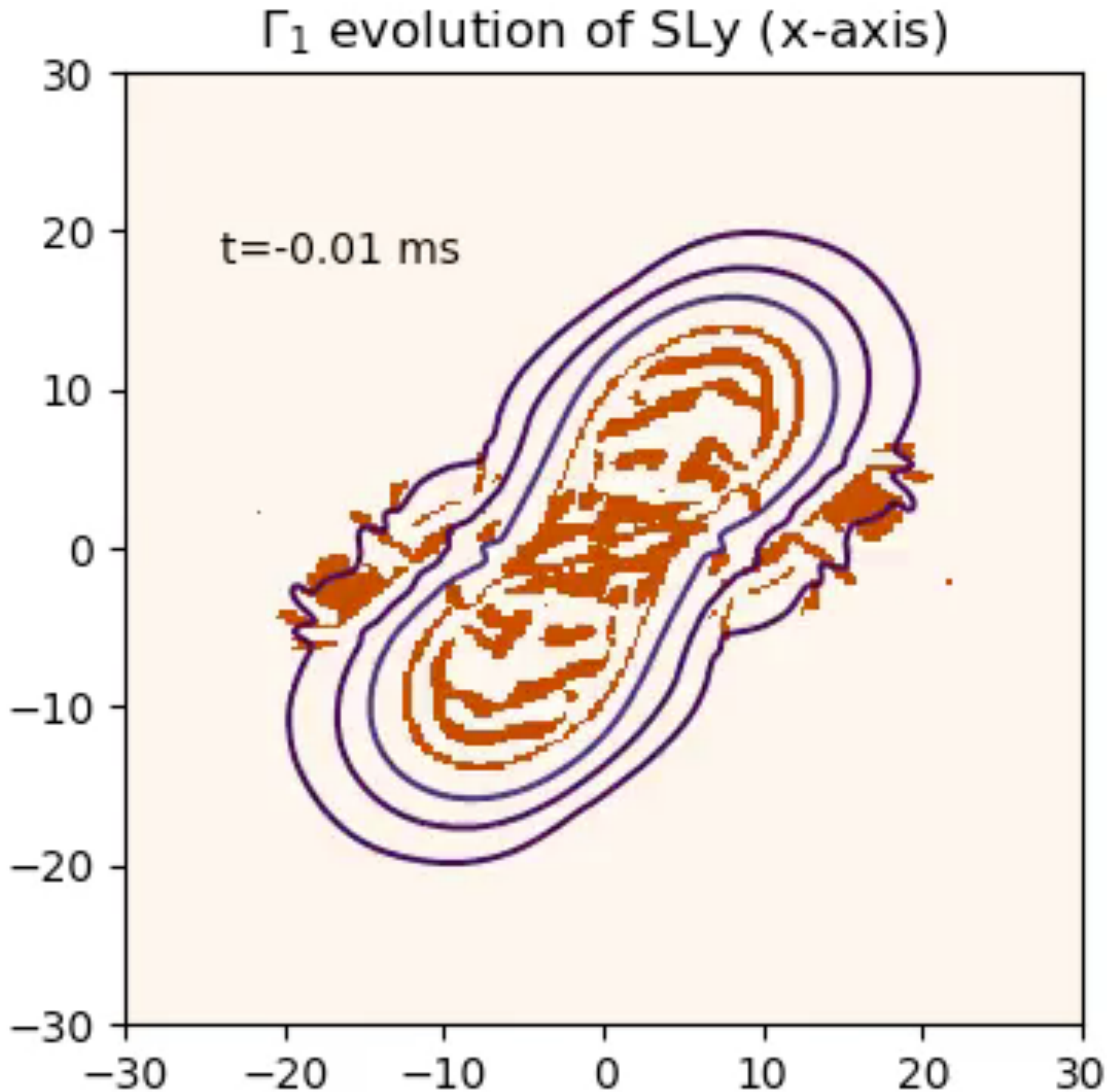

Thermal Evolution

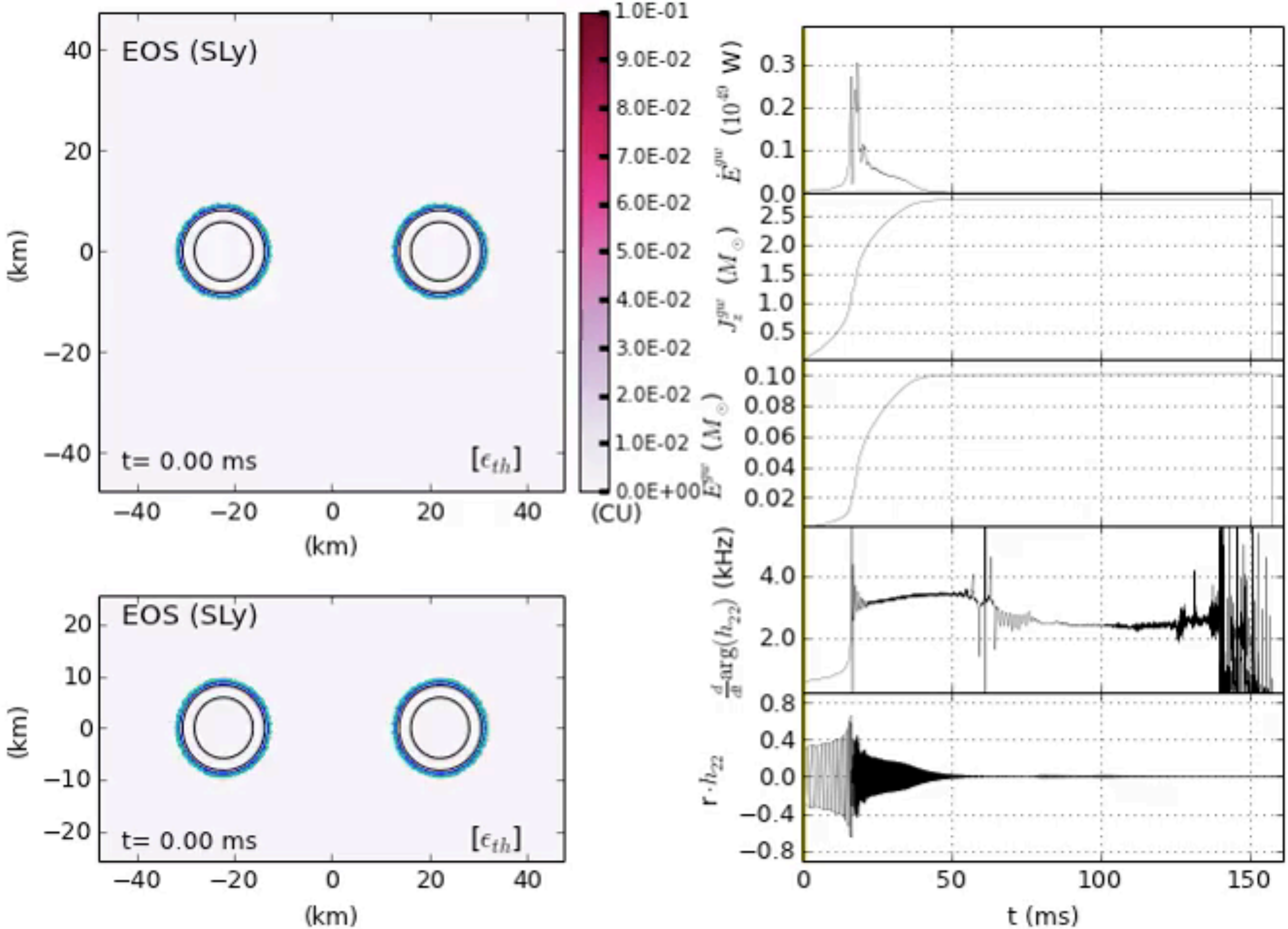

Oscillations

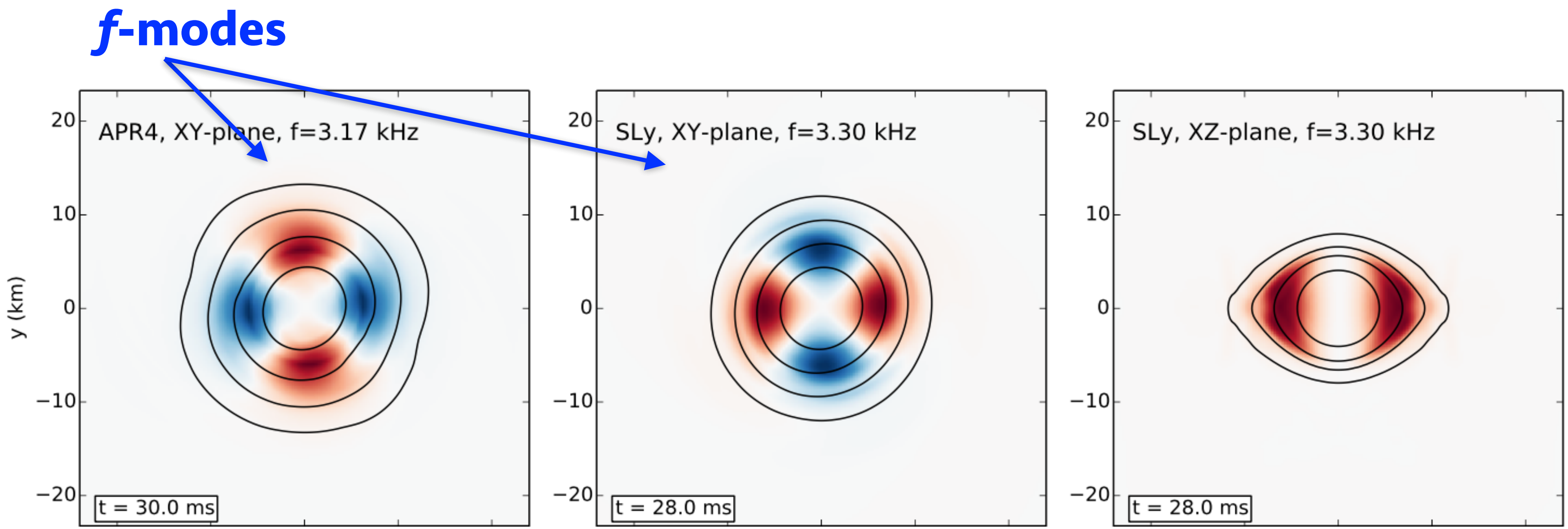

Oscillations

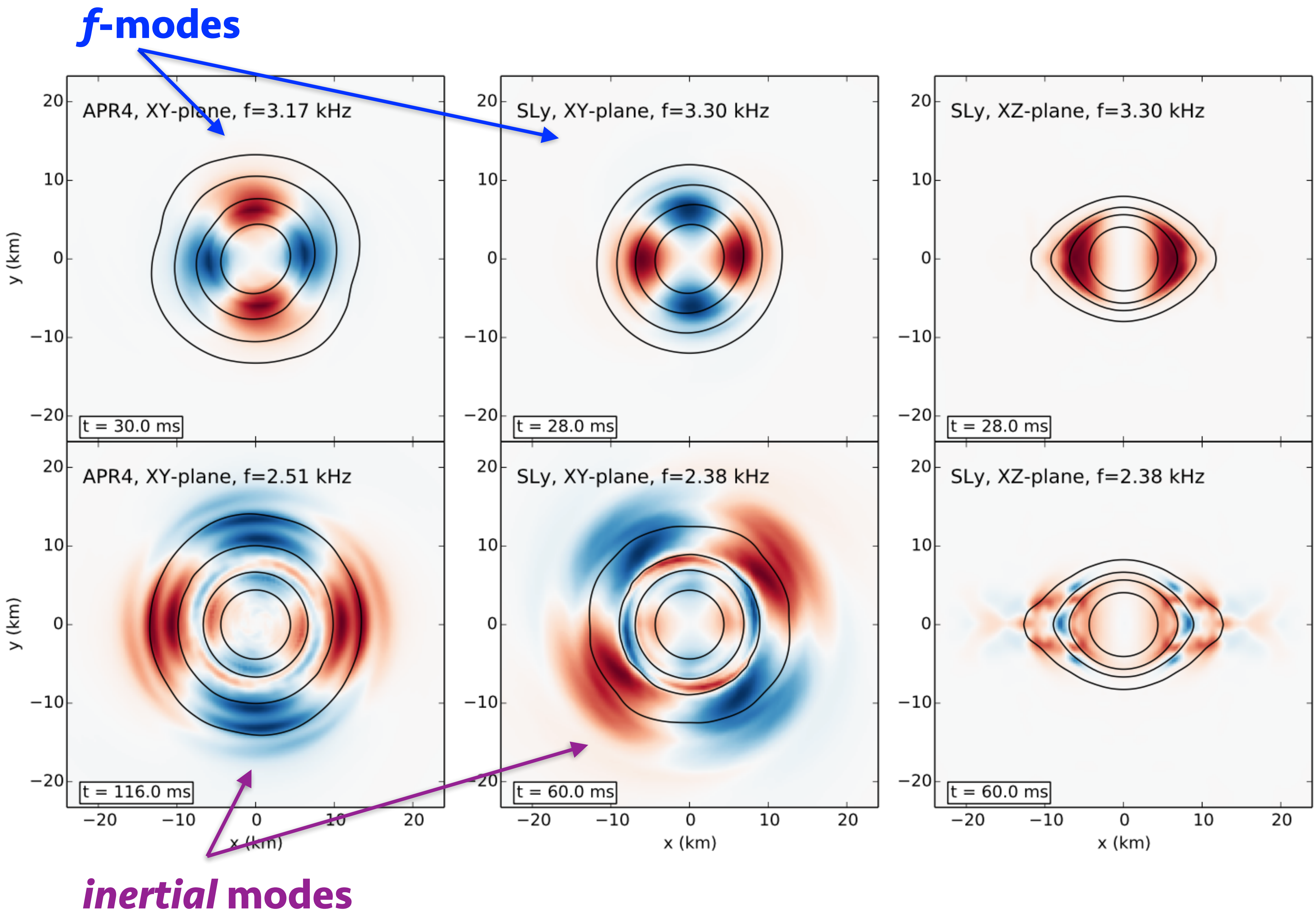

Gravitational Wave Spectrum

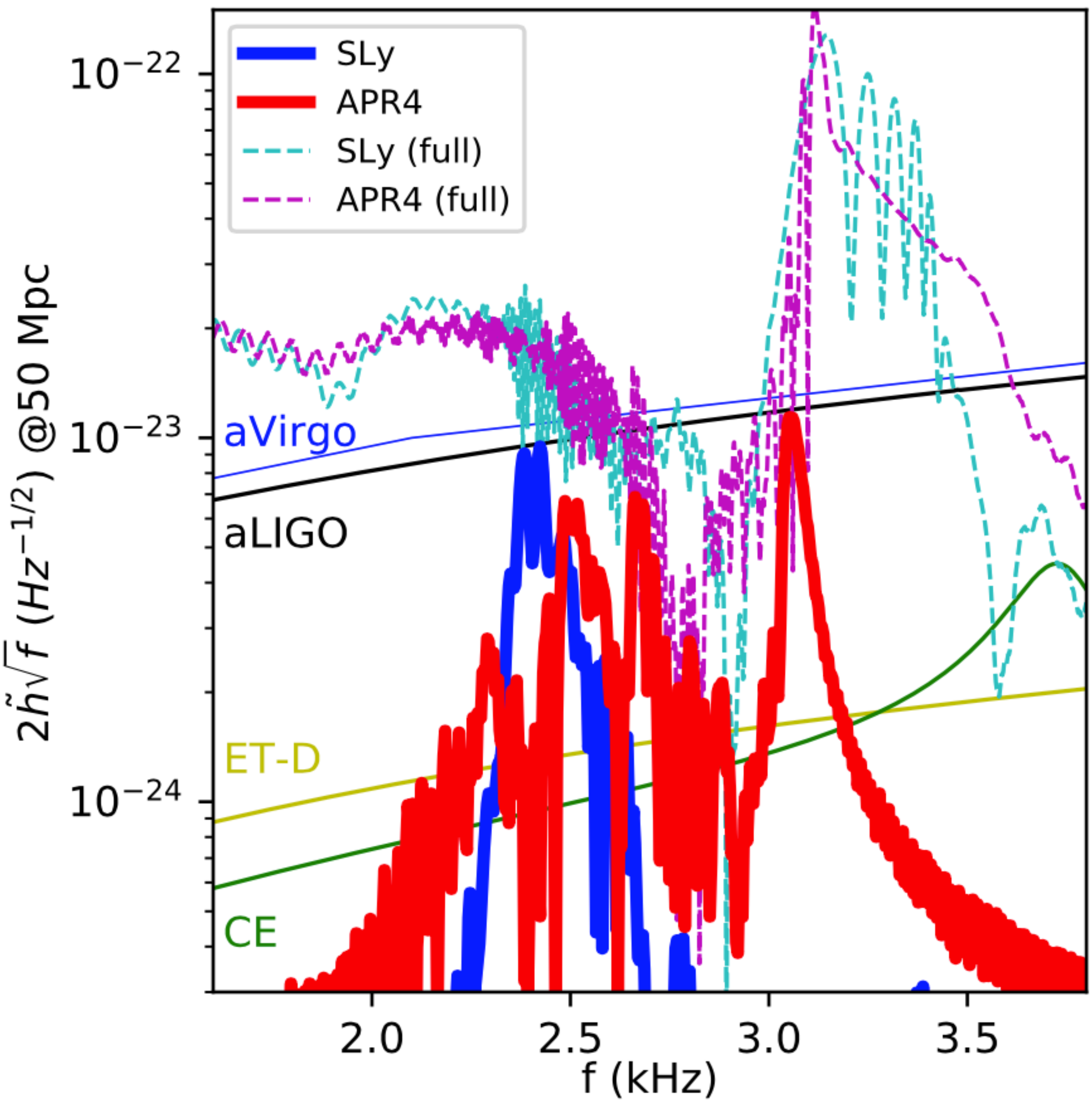

Summary

- WBased on GW170817 and causality, we set a strict minimum neutron star radius of 10.7km at 1.6M_{sun}.
- Gravitational wave asteroseismology can constraint the neutron star radius to 0.4km with future observations.
- Principal Component Analysis (PCA) sufficient to reach >90% of optimal signal.
- We discover convective instabilities and inertial modes that can probe the thermal part of the EOS.
- Once the EOS is well constrained, one can investigate departures from GR.